ARTICLE

doi:10.1038/nature22324

Maintenance of persistent activity in a frontal thalamocortical loop

Zengcai V. Guo[1]*†, Hidehiko K. Inagaki[1]*, Kayvon Daie[1], Shaul Druckmann[1], Charles R. Gerfen[2] & Karel Svoboda[1]

Persistent neural activity maintains information that connects past and future events. Models of persistent activity often invoke reverberations within local cortical circuits, but long-range circuits could also contribute. Neurons in the mouse anterior lateral motor cortex (ALM) have been shown to have selective persistent activity that instructs future actions. The ALM is connected bidirectionally with parts of the thalamus, including the ventral medial and ventral anterior–lateral nuclei. We recorded spikes from the ALM and thalamus during tactile discrimination with a delayed directional response. Here we show that, similar to ALM neurons, thalamic neurons exhibited selective persistent delay activity that predicted movement direction. Unilateral photoinhibition of delay activity in the ALM or thalamus produced contralesional neglect. Photoinhibition of the thalamus caused a short-latency and near-complete collapse of ALM activity. Similarly, photoinhibition of the ALM diminished thalamic activity. Our results show that the thalamus is a circuit hub in motor preparation and suggest that persistent activity requires reciprocal excitation across multiple brain areas.

Short-term memory is represented by changes in spike rates that are maintained internally, in the absence of sustained sensory input. Neurons in the frontal cortex show persistent activity related to different types of short-term memory[1–10]. Motor preparation is a particular short-term memory that links past events and anticipation of future movements. Motor preparation has been studied extensively using delayed-response tasks, in which a sensory stimulus instructs a future action. During the delay epoch, neurons in the motor cortex and related structures show persistent and ramping activity related to specific movements, long before movement onset[1–5,11]. We refer here to persistent activity during the delay epoch as 'preparatory activity'.

Individual neurons have time constants on the order of ten milliseconds. Persistent activity over seconds is therefore an emergent property of neural circuits, which probably involves positive feedback. Circuit models of cortical persistent activity often invoke reverberations within local circuits mediated by excitatory connections[12,13]. However, persistent activity could also arise from multi-regional interactions. Frontal and parietal cortical areas, together with associated thalamic nuclei, form a network and show persistent activity during memory-guided tasks[6,14–23]. Identifying the essential anatomical substrates for persistent activity is necessary to understand the neural mechanisms underlying short-term memory.

A large fraction of mouse ALM neurons exhibit direction-selective persistent and ramping preparatory activity in a directional licking task[3]. Preparatory activity is distributed across both ALM hemispheres[24], similar to human premotor cortex[25,26]. Three types of manipulation experiments have shown that ALM preparatory activity instructs directed licking in a tactile delayed-response task. First, unilateral inactivation of ALM during motor preparation impairs upcoming movements in the contralateral direction[3,24,27]. Second, brief unilateral activation of ALM pyramidal tract neurons has persistent effects on ALM population activity and biases the direction of future movements towards the contralateral direction[27]. Third, brief bilateral inactivation destroys selectivity of preparatory activity on average and randomizes future movements; but on a trial-by-trial basis movement direction can still be predicted on the basis of ALM population activity[24]. Preparatory activity in one hemisphere remains largely unchanged after perturbation of the other hemisphere, implying that ALM hemispheres can maintain preparatory activity independently[24]. Here we report that the maintenance of persistent activity in the ALM requires direct excitation from the thalamus and vice versa, revealing that the thalamus is a key circuit node in motor preparation.

The thalamus is required for motor preparation

Mice performed a discrimination task with a delayed response[3,27,28] (Fig. 1a, b). In each trial, mice judged the location of an object with their whiskers. During the subsequent delay epoch (1.2 or 1.3 s), mice maintained a memory of the previous sensory experience and planned an upcoming response. Following an auditory 'go' cue, mice reported object location with directional licking (left or right, mean per cent correct 77.6%; lick-early before 'go' cue 10.3%, no response 1.1%).

During the delay epoch, neurons in the ALM (centred on 2.5 mm anterior, 1.5 mm lateral[3,24]) show persistent activity that predicts licking direction (preparatory activity)[3,27]. Unilateral photoinhibition of the ALM during the delay epoch produced an ipsilateral response bias[3,27], reducing performance for contralateral trials and increasing performance for ipsilateral trials ($P < 0.001$, paired t-test; Fig. 1c). These experiments confirm that ALM preparatory activity during the delay epoch is causally involved in motor preparation[3].

Preparatory activity could be maintained by recurrent circuits within the ALM. Alternatively, additional brain areas, coupled to ALM by long-range excitatory connections, might be required. Inhibiting one of these brain areas might produce a similar behavioural bias as inhibition of the ALM. Within the cortex, the ALM forms reciprocal connections with the contralateral ALM[24,27], ipsilateral primary motor cortex (M1), and ipsilateral somatosensory cortex (Extended Data Fig. 1a, b, e). However, photoinhibition of the cortical locations outside of the ALM during the delay epoch (55 locations, covering the dorsal cortex, approximately 50% of neocortex), did not produce behavioural effects[3,24].

The ALM also makes reciprocal excitatory connections with several ipsilateral thalamic nuclei (anterior/posterior, −1.1 to −2.3 mm;

[1]Janelia Research Campus, HHMI, Ashburn, Virginia 20147, USA. [2]Laboratory of Systems Neuroscience, National Institute of Mental Health, Bethesda, Maryland 20892, USA. †Present address: School of Medicine, Tsinghua University, Beijing 100084, China.
*These authors contributed equally to this work.

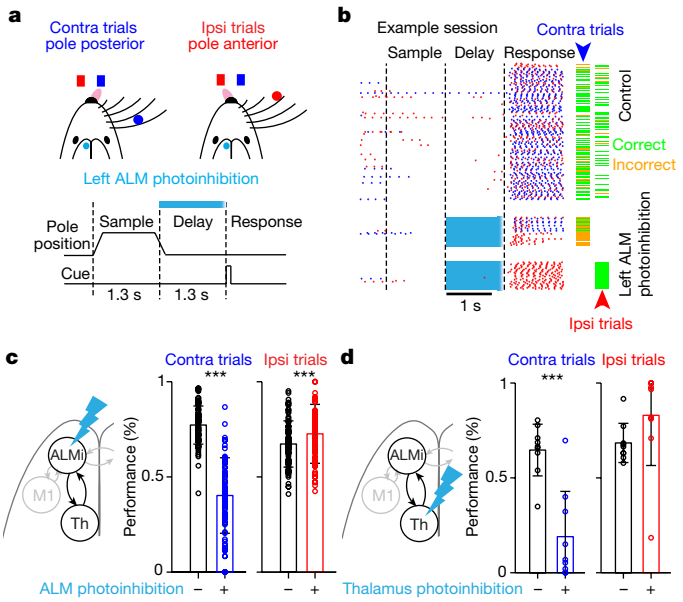

Figure 1 | The ALM and thalamus are required for motor preparation. **a**, Top, mouse reporting the location of a pole by directional licking. Contra and ipsi refer to the photoinhibited left hemisphere (cyan circle). Bottom, task structure (relevant to **b**–**d**). **b**, Example behavioural session. Blue, contra licks; red, ipsi licks. Right, trial outcome; green dash, correct; orange dash, incorrect. **c**, ALM photoinhibition. Left, schematic of photoinhibition. Right, behavioural performance. Circles, behavioural sessions ($n = 84$; 11 mice); bars, mean ± s.d.; ***$P < 0.001$, paired t-test. **d**. Same as **c** for thalamus (Th) photoinhibition ($n = 9$; 4 mice).

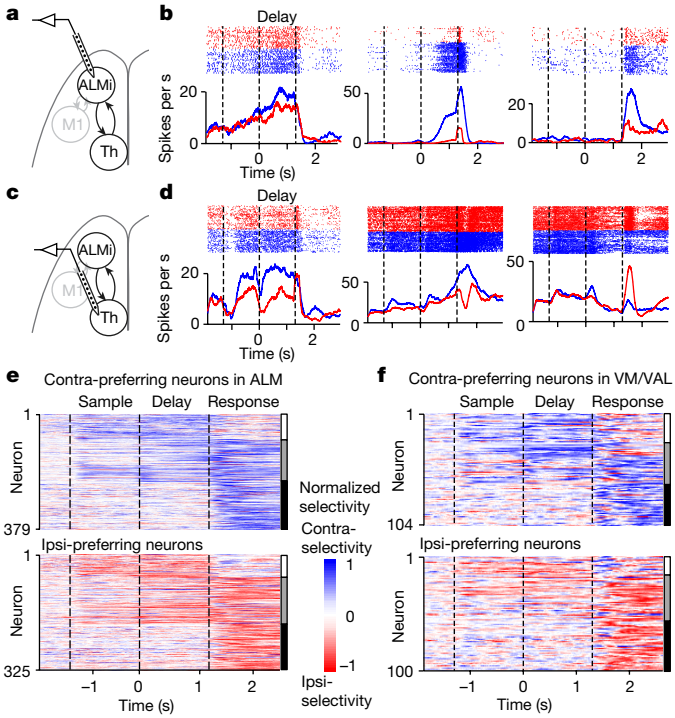

Figure 2 | The ALM and thalamus show similar neural dynamics. **a**, Silicon probe recordings in the ALM (relevant to **b**, **e**). **b**, Three example ALM neurons. Top, spike raster. Bottom, peri-stimulus time histogram. Blue, correct contra trials; red, correct ipsi trials. Dashed lines separate behavioural epochs. **c**, Silicon probe recordings in the VM/VAL (relevant to **d**, **f**). **d**, Three example VM/VAL neurons as in **b**. **e**, ALM population selectivity ($n = 704$). Vertical bars on the right; white, neurons with preparatory activity only; grey, neurons with both preparatory activity and peri-movement activity; black, neurons with peri-movement activity only. **f**, VM/VAL population selectivity ($n = 204$) as in **e**.

medial/lateral, 0–1.6 mm; dorsal/ventral, 3.3–4.8 mm relative to the bregma), including the ventral medial (VM), and parts of the ventral anterior–lateral (VAL), medial dorsal, posterior and intralaminar nuclei[19–22] (Extended Data Fig. 1c–e) (we refer to the combined thalamic nuclei that are reciprocally connected to the ALM as 'thal$_{ALM}$'). Within the thal$_{ALM}$, the VM/VAL complex was the most extensively and consistently labelled in experiments involving injections of multiple types of anterograde and retrograde tracers into the ALM (Extended Data Fig. 1f); we therefore focus inactivation experiments on the VM/VAL. However, our perturbation methods do not have sufficient resolution to exclude contributions from other thal$_{ALM}$ nuclei.

To determine whether the thalamus has a role in motor preparation, we photoinhibited the thal$_{ALM}$ during the delay epoch (Fig. 1d). We injected a Cre-dependent ChR2 (channelrhodopsin-2) virus into the thalamic reticular nucleus (TRN) of Gad2-Cre transgenic mice[29,30]. Photostimulating axonal terminals of the TRN GABAergic (γ-aminobutyric-acid-releasing) neurons in the thalamus reduced spike rates in the thal$_{ALM}$ (recorded near the VM/VAL, reduced to 67.8% during the delay epoch; Extended Data Fig. 2). Similar to the ALM, unilateral photoinhibition of the thal$_{ALM}$ during the delay epoch reduced the performance during contralateral trials and caused a small improvement in performance during ipsilateral trials ($P < 0.001$ for contralateral trials, not significant for ipsilateral trials, paired t-test; Fig. 1d).

We confirmed the behavioural effect of thal$_{ALM}$ photoinhibition using pharmacological inhibition (muscimol, 1.8–5.9 ng), which has better spatial specificity (approximately 0.5 mm)[31]. Inhibition near the VM/VAL produced an ipsilateral bias in the licking response (Extended Data Fig. 3a, b). Inhibition outside of the thal$_{ALM}$ (1.1–1.6 mm anterior or 1.6–1.9 mm dorsal to the VM/VAL) did not cause ipsilateral bias, even at tenfold higher doses (Extended Data Fig. 3c–f). Thus both the ALM and thal$_{ALM}$ are required for motor preparation.

Preparatory activity in thalamus

We recorded single units from the ALM or thal$_{ALM}$ in behaving mice. In the ALM, we focused on putative pyramidal neurons ($n = 1{,}006$ out of 1,214 neurons, 10 mice, left ALM; Extended Data Fig. 4 and Methods), because these neurons potentially project to the thal$_{ALM}$ or excite neurons that project to the thal$_{ALM}$ (Fig. 2a, b). For a majority of neurons, activity differed across trial types (70%, 704 out of 1,006; $P < 0.05$, t-test; Methods). Selectivity for movements emerged in the sample epoch, increased throughout the delay epoch, and reached a maximum at the beginning of the response epoch[3,27] (Fig. 2b, e and Extended Data Fig. 4c). ALM neuron responses were diverse: subsets of neurons showed selective preparatory activity (Fig. 2b (left), e, 145 out of 1,006), selective peri-movement activity during the response epoch (Fig. 2b (right), e, 272 out of 1,006), or both (Fig. 2b (middle), e, 287 out of 1,006). Approximately equal numbers of neurons preferred contra- or ipsilateral movements (Fig. 2e), consistent with previous recordings[3,4,27].

We next recorded single units from the left thalamus ($n = 790$; 11 mice) (Fig. 2c, d). A subset of these units ($n = 295$) were in the VM/VAL, with the others in the surrounding thalamus outside of the thal$_{ALM}$ (Extended Data Fig. 4). A majority of VM/VAL neurons discriminated trial types (69%, 204 out of 295; indistinguishable from the ALM, χ^2 test, $P = 0.79$). Selectivity emerged in the sample epoch, increased throughout the delay epoch, and reached a maximum during the response epoch (Fig. 2d, f and Extended Data Fig. 4f). VM/VAL neurons exhibited a similar selectivity and time course to the ALM (χ^2 test, $P > 0.5$): subsets of neurons showed selective preparatory activity (Fig. 2d (left), f, 43 out of 295 neurons), selective peri-movement activity during the response epoch (Fig. 2d (right), f, 82 out of 295), or both (Fig. 2d (middle), f, 79 out of 295). VM/VAL neurons therefore showed similar preparatory activity to ALM neurons.

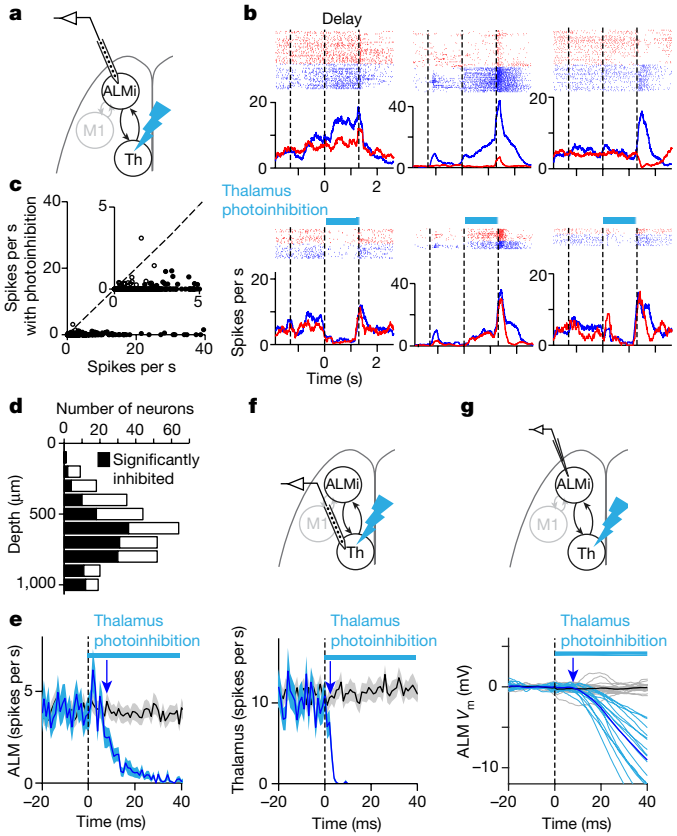

Figure 3 | The thalamus drives the ALM. **a**–**e**, Recording in the ALM during thalamus photoinhibition. **a**, Schematic. **b**, Three example neurons as in Fig. 2b. **c**, Spike rates during 20–120 ms after photostimulus onset. Filled circles, neurons that were significantly modulated by thalamus photoinhibition ($P < 0.05$, t-test); dotted line, unity line. Inset, blow-up of the scatter plot. **d**, Number of modulated ALM neurons across cortical depth. **e**, Average time course of ALM neurons during thalamus photoinhibition. Black, control peri-stimulus time histogram; blue, photoinhibition ($n = 314$). Shading, s.e.m. Arrow, onset of ALM inhibition. **f**, Top, recording in the thalamus during thalamus photoinhibition. Bottom, average time course of thalamic neurons ($n = 148$) as in **e**. **g**, Top, whole-cell recording in the ALM during thalamus photoinhibition. Bottom, thick lines, time course of mean V_m (black, control; dark blue, photoinhibition) ($n = 16$ cells). Thin lines (grey, control; light blue, photoinhibition), time course of individual neurons.

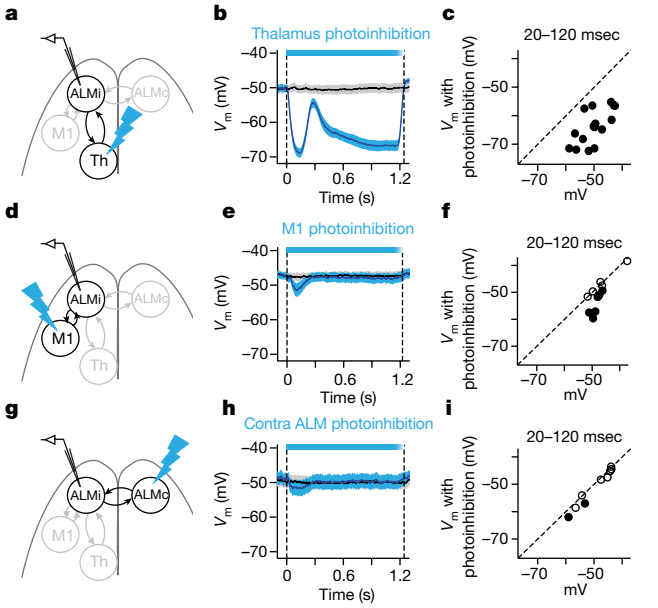

Figure 4 | Comparison of thalamic and cortical input. **a**–**c**, Whole-cell recording in the ALM during thalamus photoinhibition ($n = 16$ cells). **d**–**f**, Whole-cell recording in the ALM during M1 photoinhibition ($n = 11$ cells). **g**–**i**, Whole-cell recording in the ALM during contralateral ALM photoinhibition ($n = 9$ cells). **a**, **d**, **g**, Schematic. **b**, **e**, **h**, Time course of mean V_m in ALM neurons during thalamus (**b**), M1 (**e**) or contra ALM (**h**) photoinhibition. Shading, s.e.m. **b**, Two hundred milliseconds after photostimulation onset, the V_m transiently recovered, probably caused by a concomitant rebound in $thal_{ALM}$ activity (Extended Data Fig. 2). **c**, **f**, **i**, Mean V_m during 20–120 ms after photostimulus onset. Filled circles, neurons that were significantly modulated by photoinhibition ($P < 0.05$, t-test); dotted line, the unity line.

The thalamus drives ALM preparatory activity

Our behavioural and electrophysiological data show that the ALM and $thal_{ALM}$ contribute to motor preparation. We therefore investigated whether ALM preparatory activity is influenced by the $thal_{ALM}$, or vice versa. We recorded from ALM neurons while photoinhibiting the ipsilateral $thal_{ALM}$ (Fig. 3a, Extended Data Fig. 2 and Methods). We photostimulated GABAergic axons near the $thal_{ALM}$, using VGAT–ChR2–EYFP mice[3,32] in which a larger fraction of GABAergic axons express ChR2, compared to virus-injected mice. Photoinhibition abolished $thal_{ALM}$ activity nearly completely (to 2% of control without photoinhibition) (Fig. 3f) and indirectly also the activity of ALM neurons (Fig. 3b–e). We measured ALM activity for 100 ms, starting 20 ms after light onset of $thal_{ALM}$ photoinhibition; this time window excludes the subsequent transient rebound activity in the $thal_{ALM}$ and ALM observed during prolonged photoinhibition (Extended Data Fig. 2). $Thal_{ALM}$ photoinhibition decreased ALM activity to 6% of control, reducing activity in nearly all neurons (Fig. 3c, 309 out of 314 inhibited, 3 out of 314 activated, 155 out of 314 significantly inhibited, 0 out of 314 significantly activated, t-test, $P < 0.05$), across all cortical layers (Fig. 3d) (neurons showing preparatory activity, peri-movement selectivity or both were equally inhibited; Fig. 3b, $P > 0.2$, t-test).

Compared to extracellular recordings, membrane potential (V_m) measurements provide a more precise time course of the effects of $thal_{ALM}$ photoinhibition in the ALM. In addition, V_m recordings can distinguish a decrease in excitation from an increase in inhibition as proximal cause for the collapse of ALM activity[33]. Whole-cell recordings revealed that the average V_m of ALM neurons was close to the spike threshold during the delay epoch (action potential threshold − mean basal $V_m = 12.7 \pm 0.7$ mV (mean ± s.e.m.) $n = 60$ cells), consistent with the relatively high spike rates in the ALM. $Thal_{ALM}$ photoinhibition caused hyperpolarization (V_m control trials − V_m photoinhibition trials $= 18.7 \pm 1.1$ mV (mean ± s.e.m.); measured for 100 ms, starting 20 ms after photostimulus onset; $n = 16$ cells), preventing ALM neurons from spiking (Figs 3g, 4b and Extended Data Fig. 5a, b). Manipulating the V_m during recording revealed that hyperpolarization was mainly caused by a reduction in excitation, not an increase in inhibition (Extended Data Fig. 5c–n). This implies that the $thal_{ALM}$ is a major driver of ALM neurons.

We explored whether the decrease in ALM activity is a direct consequence of loss of input from the $thal_{ALM}$. Given that thalamic areas near the $thal_{ALM}$ project to the M1, ALM activity could be affected through the thalamus→M1→ALM pathway. First, we computed the time between loss of $thal_{ALM}$ activity and reduction in ALM activity (latency difference). Photoinhibition reduced $thal_{ALM}$ activity 2.5 ± 0.8 ms after photostimulus onset (mean ± s.e.m., activity reduction onset detected by 3 s.d., Fig. 3f). Hyperpolarization of ALM neurons and reduction of ALM spike rates were detected 7.9 ± 1.7 ms and 8.2 ± 1.5 ms after photostimulus onset, respectively (mean ± s.e.m., Fig. 3e, g). The latency difference, 5.4 ms, is explained by the $thal_{ALM}$→ALM conduction delay (3.6 ± 1.1 ms) and the delay caused by the time constant of ALM neurons (at least 1.8 ± 0.7 ms; Extended Data Fig. 6 and Supplementary Information). The thalamus→M1→ALM pathway would produce a latency difference of more than 14.3 ms, too

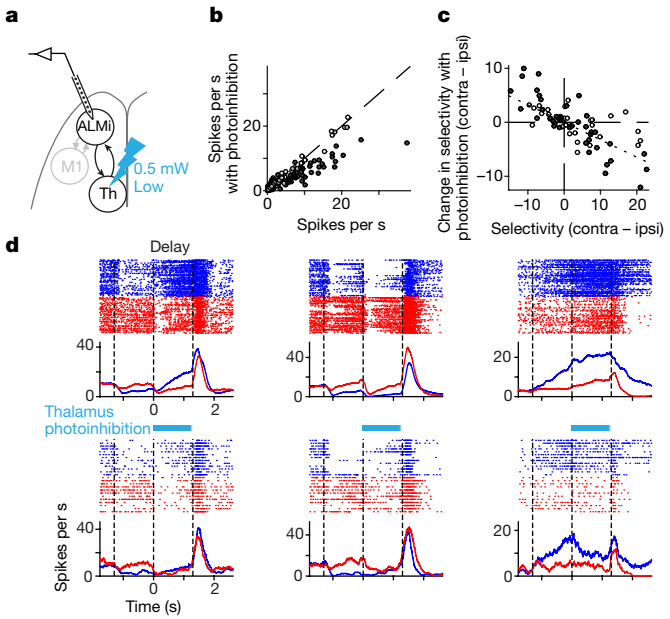

Figure 5 | Thalamic activity maintains selectivity in the ALM. **a**–**d**, Recording in the ALM during low thalamic photoinhibition. **a**, Schematic. **b**, Spike rates were measured for 1,300 ms during photoinhibition and control conditions. Filled circles, neurons that were significantly modulated by thalamus photoinhibition ($P < 0.05$, t-test, $n = 160$). **c**, Relationship between selectivity of individual neurons and changes in selectivity due to photoinhibition of the thalamus. Dotted line, linear regression (slope = −0.33, Pearson correlation coefficient = −0.75). Filled circles, as in **b**. **d**, Three example neurons as in Fig. 2b.

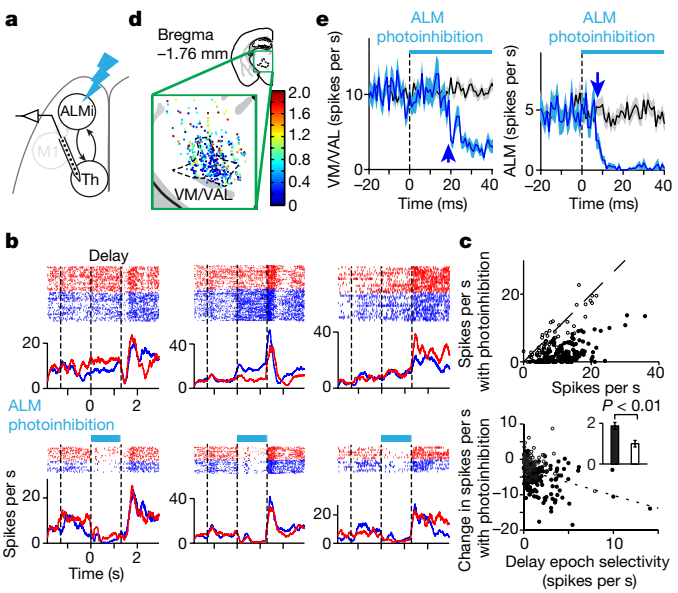

Figure 6 | The ALM drives the thalamus. **a**–**e**, Recording in the VM/VAL during ALM photoinhibition. **a**, Schematic. **b**, Three example neurons as in Fig. 2b. **c**, Top, spike rates during 20–120 ms after photostimulus onset. Bottom, relationship between change of spike rates due to photoinhibition and delay epoch selectivity. Filled circles (top and bottom), neurons that were significantly modulated by ALM photoinhibition ($P < 0.05$, t-test); Dotted line, unity line (top) or linear regression (bottom; slope = −0.73, Pearson correlation coefficient = −0.33). Inset, delay epoch selectivity of significantly (black bar) and non-significantly (white bar) modulated neurons ($P = 0.002$, t-test). **d**, Locations of recorded neurons in the thalamus. Neurons were colour-coded on the basis of their spike rate during ALM photoinhibition normalized to the spike rate without ALM photoinhibition (Methods). **e**, Left, time course of VM/VAL activity during ALM photoinhibition ($n = 201$ neurons). Right, time course of activity in ALM pyramidal neurons during ALM photoinhibition ($n = 256$ neurons) as in Fig. 3e.

slow by more than 9 ms to explain the hyperpolarization in the ALM (Extended Data Fig. 6).

Second, direct photoinhibition of the M1 during the delay epoch (silencing more than 90% of the spikes in a cortical area with a radius of 1 mm, Methods) caused only a slight hyperpolarization of the V_m and decreased spike rates of ALM neurons (−3.3 ± 1.0 mV; −1.4 ± 0.6 spikes per s (mean ± s.e.m.), $n = 11$ cells) (Fig. 4d–f). These findings imply that the $thal_{ALM} \rightarrow M1 \rightarrow ALM$ pathway cannot explain V_m changes in the ALM during $thal_{ALM}$ photoinhibition. We conclude that the $thal_{ALM}$ drives the ALM directly.

We tested whether the coupling between the ALM and $thal_{ALM}$ is stronger than coupling with other reciprocally connected structures (Extended Data Fig. 1d). Photoinhibiting M1, including a large number of ALM-projecting neurons, had a negligible effect on ALM activity (Fig. 4d–f). Similarly, photoinhibiting the contralateral ALM, the anatomically strongest input to the ALM, hardly changed the V_m (−1.4 ± 0.5 mV (mean ± s.e.m.), $n = 9$ cells) and had little effect on preparatory activity[24] (Fig. 4g–i). Together, the $thal_{ALM}$ drives the ALM directly and more strongly than other reciprocally connected structures (compare Fig. 4b and 4e, h).

The thalamus contributes to selectivity in the ALM

We asked whether the $thal_{ALM}$ contributes to selectivity in the ALM or is simply required to maintain the spike rates in the ALM without affecting selectivity. Strong silencing (as in Figs 3, 4) of the thalamus abolished ALM activity, making it difficult to quantify the contribution of the thalamus to ALM selectivity. However, we noticed that the few neurons that maintained activity after $thal_{ALM}$ silencing lost selectivity (for example, Fig. 3b (neuron 2)). We therefore searched for conditions where photoinhibition of $thal_{ALM}$ had moderate effects on activity but larger effects on selectivity. We used 20-fold lower photostimuli compared to the experiments in Figs 3, 4 (stimulating in VGAT–ChR2–EYFP mice, 0.5 mW, 473 nm light). During low photoinhibition, 83 out of 160 of ALM neurons showed statistically significant changes in mean spike rate (t-test; average reduction in spike rate, 1.2 ± 0.2 spikes per s (mean ± s.e.m.), $n = 160$; Fig. 5a, b). A substantial fraction of these neurons (39%, 32 out of 83) showed increases in spike rate, inconsistent with the thalamus providing a uniform additive drive to ALM.

This unequal spike rate change reduced the selectivity of ALM neurons in both contra- and ipsi-preferring neurons (Fig. 5c, d and Extended Data Fig. 7a, b). A reduction in selectivity was seen even for neurons that did not show a change in mean spike rate (for example, Fig. 5c (white circles), d (cell 2)). Together, these results support the idea that the thalamus is necessary to maintain ALM spike rates and selectivity during motor preparation.

We implemented network models of selective persistent activity (Extended Data Fig. 7c–e and Supplementary Information). Our data are inconsistent with linear models with either specific (like-to-like) or non-specific (all-to-all) thalamocortical connectivity. However, our data do not exclude nonlinear models with specific or non-specific thalamocortical connectivity (Extended Data Fig. 7d). Methods to manipulate thalamic neurons differentially based on their selectivity will be required to distinguish between architectures of nonlinear models.

The ALM drives thalamic preparatory activity

We next investigated whether $thal_{ALM}$ activity is influenced by ALM. We recorded from VM/VAL neurons while photoinhibiting the ipsilateral ALM during the delay epoch (Fig. 6a). Photoinhibition of the ALM decreased the activity of VM/VAL neurons (Fig. 6b). VM/VAL neurons selective during sample, delay or response epochs were equally inhibited (Fig. 6b, $P > 0.2$, t-test). We measured activity for 100 ms, starting 20 ms after photostimulus onset. ALM photoinhibition decreased activity in a majority of VM/VAL neurons (to 25% of control; 190 out of 201 inhibited, 11 out of 201 activated, 139 out of 201 significantly

inhibited, 0 out of 201 significantly activated, $P < 0.05$, t-test, Fig. 6c). This reduction in activity was mainly limited to VM/VAL (Fig. 6d and Extended Data Fig. 8a–c) in the vicinity of ALM projections (Extended Data Fig. 1).

A small fraction of neurons in VM/VAL was not changed by ALM photoinhibition. These neurons also showed significantly less selectivity (Fig. 6c, $P = 0.002$, t-test). By contrast, VM/VAL neurons with strongly reduced activity after ALM photoinhibition carried trial-type information (Fig. 6c). This suggests that selectivity in VM/VAL requires ALM input.

We next determined whether the reduction in $thal_{ALM}$ activity is caused by loss of excitation from ALM pyramidal neurons. We considered three alternatives. First, photoinhibiting the nearby vibrissal primary motor cortex (vM1), which projects to parts of the VAL, did not cause a reduction in $thal_{ALM}$ activity (Extended Data Fig. 8d–g), excluding the ALM →vM1→ $thal_{ALM}$ pathway. Second, GABAergic neurons in the ALM do not project to the $thal_{ALM}$ (Extended Data Fig. 8h, i), excluding direct photoinhibition of the $thal_{ALM}$.

Third, the basal ganglia nucleus substantia nigra reticulata (SNr) inhibits the $thal_{ALM}$ through GABAergic projections[34] (Extended Data Fig. 9). The ALM could potentially decrease $thal_{ALM}$ activity by increasing the activity of SNr neurons through the striatum or subthalamic nucleus[34]. However, recordings from SNr neurons during ALM photoinhibition argue against this possibility (Extended Data Fig. 10 and Methods). Together, these experiments imply that the ALM drives the VM/VAL directly.

Discussion

Local recurrent connectivity is often invoked as a mechanism for persistent activity[12,13,35]. Our results show that persistent preparatory activity cannot be sustained by recurrent excitation within cortical circuits alone[29], but in addition require recurrent excitation through a thalamocortical loop. Inactivation of the $thal_{ALM}$ resulted in strong hyperpolarization of ALM neurons. The mechanisms underlying this powerful driving influence of the $thal_{ALM}$ on the ALM, compared to the influence of cortical areas, represent an important area for future investigation.

We further identify the frontal cortex (ALM) as a major source of driving excitation to the higher-order thalamus ($thal_{ALM}$)[36–38]. The thalamus also receives input from the deep cerebellar nuclei, the superior colliculus and the SNr (Extended Data Fig. 9), and these subcortical structures in turn receive direct or indirect input from the ALM[27]. The precise roles of these more complex loops during motor preparation and movement initiation remain to be elucidated[37,39]. Thalamus may work as a hub to convey subcortical signals to the ALM.

Besides the VM/VAL, ALM interacts with the posterior, intralaminar and midline thalamic nuclei (Extended Data Fig. 1). These nuclei project axons widely across the cerebral cortex and have been implicated in attention, awareness, arousal, consciousness, memory, voluntary movements and other functions[40–43]. Dissecting the distinct roles of these different nuclei will require manipulating specific nuclei using molecular methods. Given the widespread reciprocal connectivity between the frontal cortex and thalamus[20,21,44], persistent activity in cortical areas outside of the ALM in different behavioural contexts probably also depends on thalamocortical loops.

Online Content Methods, along with any additional Extended Data display items and Source Data, are available in the online version of the paper; references unique to these sections appear only in the online paper.

Received 7 October 2016; accepted 3 April 2017.
Published online 3 May 2017.

1. Tanji, J. & Evarts, E. V. Anticipatory activity of motor cortex neurons in relation to direction of an intended movement. *J. Neurophysiol.* **39,** 1062–1068 (1976).
2. Churchland, M. M., Cunningham, J. P., Kaufman, M. T., Ryu, S. I. & Shenoy, K. V. Cortical preparatory activity: representation of movement or first cog in a dynamical machine? *Neuron* **68,** 387–400 (2010).
3. Guo, Z. V. *et al.* Flow of cortical activity underlying a tactile decision in mice. *Neuron* **81,** 179–194 (2014).
4. Erlich, J. C., Bialek, M. & Brody, C. D. A cortical substrate for memory-guided orienting in the rat. *Neuron* **72,** 330–343 (2011).
5. Murakami, M., Vicente, M. I., Costa, G. M. & Mainen, Z. F. Neural antecedents of self-initiated actions in secondary motor cortex. *Nat. Neurosci.* **17,** 1574–1582 (2014).
6. Fuster, J. M. & Alexander, G. E. Neuron activity related to short-term memory. *Science* **173,** 652–654 (1971).
7. Funahashi, S., Bruce, C. J. & Goldman-Rakic, P. S. Mnemonic coding of visual space in the monkey's dorsolateral prefrontal cortex. *J. Neurophysiol.* **61,** 331–349 (1989).
8. Romo, R., Brody, C. D., Hernández, A. & Lemus, L. Neuronal correlates of parametric working memory in the prefrontal cortex. *Nature* **399,** 470–473 (1999).
9. Liu, D. *et al.* Medial prefrontal activity during delay period contributes to learning of a working memory task. *Science* **346,** 458–463 (2014).
10. Wang, X. J. Decision making in recurrent neuronal circuits. *Neuron* **60,** 215–234 (2008).
11. Maimon, G. & Assad, J. A. A cognitive signal for the proactive timing of action in macaque LIP. *Nat. Neurosci.* **9,** 948–955 (2006).
12. Goldman-Rakic, P. S. Cellular basis of working memory. *Neuron* **14,** 477–485 (1995).
13. Wang, X. J. Synaptic reverberation underlying mnemonic persistent activity. *Trends Neurosci.* **24,** 455–463 (2001).
14. Zingg, B. *et al.* Neural networks of the mouse neocortex. *Cell* **156,** 1096–1111 (2014).
15. Crutcher, M. D. & Alexander, G. E. Movement-related neuronal activity selectively coding either direction or muscle pattern in three motor areas of the monkey. *J. Neurophysiol.* **64,** 151–163 (1990).
16. Gnadt, J. W. & Andersen, R. A. Memory related motor planning activity in posterior parietal cortex of macaque. *Exp. Brain Res.* **70,** 216–220 (1988).
17. Bruce, C. J. & Goldberg, M. E. Primate frontal eye fields. I. Single neurons discharging before saccades. *J. Neurophysiol.* **53,** 603–635 (1985).
18. Hernández, A. *et al.* Decoding a perceptual decision process across cortex. *Neuron* **66,** 300–314 (2010).
19. Herkenham, M. The afferent and efferent connections of the ventromedial thalamic nucleus in the rat. *J. Comp. Neurol.* **183,** 487–517 (1979).
20. Oh, S. W. *et al.* A mesoscale connectome of the mouse brain. *Nature* **508,** 207–214 (2014).
21. Hunnicutt, B. J. *et al.* A comprehensive thalamocortical projection map at the mesoscopic level. *Nat. Neurosci.* **17,** 1276–1285 (2014).
22. Kuramoto, E. *et al.* Ventral medial nucleus neurons send thalamocortical afferents more widely and more preferentially to layer 1 than neurons of the ventral anterior–ventral lateral nuclear complex in the rat. *Cereb. Cortex* **25,** 221–235 (2015).
23. Tanaka, M. Cognitive signals in the primate motor thalamus predict saccade timing. *J. Neurosci.* **27,** 12109–12118 (2007).
24. Li, N., Daie, K., Svoboda, K. & Druckmann, S. Robust neuronal dynamics in premotor cortex during motor planning. *Nature* **532,** 459–464 (2016).
25. Shibasaki, H. & Hallett, M. What is the Bereitschaftspotential? *Clin. Neurophysiol.* **117,** 2341–2356 (2006).
26. Fried, I., Mukamel, R. & Kreiman, G. Internally generated preactivation of single neurons in human medial frontal cortex predicts volition. *Neuron* **69,** 548–562 (2011).
27. Li, N., Chen, T. W., Guo, Z. V., Gerfen, C. R. & Svoboda, K. A motor cortex circuit for motor planning and movement. *Nature* **519,** 51–56 (2015).
28. Guo, Z. V. *et al.* Procedures for behavioral experiments in head-fixed mice. *PLoS One* **9,** e88678 (2014).
29. Reinhold, K., Lien, A. D. & Scanziani, M. Distinct recurrent versus afferent dynamics in cortical visual processing. *Nat. Neurosci.* **18,** 1789–1797 (2015).
30. Wimmer, R. D. *et al.* Thalamic control of sensory selection in divided attention. *Nature* **526,** 705–709 (2015).
31. Krupa, D. J., Ghazanfar, A. A. & Nicolelis, M. A. Immediate thalamic sensory plasticity depends on corticothalamic feedback. *Proc. Natl Acad. Sci. USA* **96,** 8200–8205 (1999).
32. Zhao, S. *et al.* Cell type-specific channelrhodopsin-2 transgenic mice for optogenetic dissection of neural circuitry function. *Nat. Methods* **8,** 745–752 (2011).
33. Yu, J., Gutnisky, D. A., Hires, S. A. & Svoboda, K. Layer 4 fast-spiking interneurons filter thalamocortical signals during active somatosensation. *Nat. Neurosci.* **19,** 1647–1657 (2016).
34. Yin, H. H. & Knowlton, B. J. The role of the basal ganglia in habit formation. *Nat. Rev. Neurosci.* **7,** 464–476 (2006).
35. Mante, V., Sussillo, D., Shenoy, K. V. & Newsome, W. T. Context-dependent computation by recurrent dynamics in prefrontal cortex. *Nature* **503,** 78–84 (2013).
36. Goldberg, J. H. & Fee, M. S. A cortical motor nucleus drives the basal ganglia-recipient thalamus in singing birds. *Nat. Neurosci.* **15,** 620–627 (2012).
37. Goldberg, J. H., Farries, M. A. & Fee, M. S. Basal ganglia output to the thalamus: still a paradox. *Trends Neurosci.* **36,** 695–705 (2013).
38. Sherman, S. M. & Guillery, R. W. *Functional Connections of Cortical Areas: a New View from the Thalamus.* (MIT Press, 2013).

39. Duan, C. A., Erlich, J. C. & Brody, C. D. Requirement of prefrontal and midbrain regions for rapid executive control of behavior in the rat. *Neuron* **86,** 1491–1503 (2015).
40. Van der Werf, Y. D., Witter, M. P. & Groenewegen, H. J. The intralaminar and midline nuclei of the thalamus. Anatomical and functional evidence for participation in processes of arousal and awareness. *Brain Res. Rev.* **39,** 107–140 (2002).
41. Saalmann, Y. B. Intralaminar and medial thalamic influence on cortical synchrony, information transmission and cognition. *Front. Syst. Neurosci.* **8,** 83 (2014).
42. Giber, K. *et al.* A subcortical inhibitory signal for behavioral arrest in the thalamus. *Nat. Neurosci.* **18,** 562–568 (2015).
43. Isseroff, A., Rosvold, H. E., Galkin, T. W. & Goldman-Rakic, P. S. Spatial memory impairments following damage to the mediodorsal nucleus of the thalamus in rhesus monkeys. *Brain Res.* **232,** 97–113 (1982).
44. Parnaudeau, S. *et al.* Inhibition of mediodorsal thalamus disrupts thalamofrontal connectivity and cognition. *Neuron* **77,** 1151–1162 (2013).

Supplementary Information is available in the online version of the paper.

Acknowledgements We thank N. Li, J. Yu, J. Goldberg, X.-J. Wang, A. Hantman, J. Phillips, G. Shepherd and N. Yamawaki for comments on the manuscript, L. Walendy, T. Pluntke and M. Inagaki for animal training, T. Harris, B. Barbarits, J. J. Jun and W.-L. Sun for help with silicon probe recordings and spike sorting, M. Economo for help with image processing and A. Hu for help with histology. This work was funded by the Howard Hughes Medical Institute. H.K.I. and K.D. are Helen Hay Whitney Foundation postdoctoral fellows. K.D. is supported by the Simons Collaboration on the Global Brain.

Author Contributions Z.V.G., H.K.I. and K.S. conceived the project. Z.V.G. and H.K.I. performed extracellular electrophysiology and optogenetic experiments. H.K.I. performed whole-cell recordings. Z.V.G., H.K.I. and C.R.G. performed anatomical experiments. K.D. and S.D. performed network modelling. Z.V.G., H.K.I. and K.S. analysed data. Z.V.G., H.K.I. and K.S. wrote the paper, with input from all the authors.

Author Information Reprints and permissions information is available at www.nature.com/reprints. The authors declare no competing financial interests. Readers are welcome to comment on the online version of the paper. Publisher's note: Springer Nature remains neutral with regard to jurisdictional claims in published maps and institutional affiliations. Correspondence and requests for materials should be addressed to K.S. (svobodak@janelia.hhmi.org).

Reviewer Information *Nature* thanks D. J. Simons and the other anonymous reviewer(s) for their contribution to the peer review of this work.

METHODS

Mice. This study is based on data from 71 mice (age > postnatal day (P)60, we used both male and female mice) (Supplementary Tables 1, 2). We used six transgenic mouse lines: PV-IRES-Cre[45], Ai32 (Rosa-CAG-LSL-ChR2(H134R)-EYFP-WPRE, JAX 012569)[46], VGAT–ChR2–EYFP[32], Gad2-IRES-Cre (a gift from B. Zemelman), Ai35D (Rosa-CAG-LSL-Arch-GFP-WPRE, JAX 012735)[46], and Olig3-Cre[47].

All procedures were in accordance with protocols approved by the Janelia Institutional Animal Care and Use Committee. Detailed information on water restriction, surgical procedures and behaviour have been published[3,28]. All surgical procedures were carried out aseptically under 1–2% isoflurane anaesthesia. Buprenorphine HCl (0.1 mg kg^{-1}, intraperitoneal injection; Bedford Laboratories) was used for postoperative analgesia. Ketoprofen (5 mg kg^{-1}, subcutaneous injection; Fort Dodge Animal Health) was used at the time of surgery and postoperatively to reduce inflammation. After the surgery, mice were allowed free access to water for at least three days before the start of water restriction. Mice were housed in a 12:12 reverse light:dark cycle and behaviourally tested during the dark phase. A typical behavioural session lasted 1–2 h and mice obtained all of their water in the behaviour apparatus (approximately 1 ml per day; 0.3 ml was supplemented if mice drank less than 0.5 ml). On other days mice received 1 ml water per day.

Mice were implanted with a titanium headpost[28]. For ALM photoinhibition, mice were implanted with a clear skull cap[3]. Optical fibres for photostimulation or cannulae for muscimol infusion were implanted during the headpost surgery or after behavioural training. Craniotomies for recording were made after behavioural training. All coordinates are given with respect to bregma (anterior–posterior (AP), medial–lateral (ML), dorso–ventral (DV)).

Behaviour. A metal pole (diameter, 0.9 mm) was presented in one of two locations[3,28] (Fig. 1). The two pole locations were 8.58 mm apart along the anterior–posterior axis. The posterior pole position was 5 mm from the whisker pad. Whiskers made contacts with the object at both pole locations, more strongly in the posterior location. A two-spout lickport (4.5 mm between spouts) was used to record licking events and deliver water rewards.

At the beginning of each trial, the pole moved within reach of the whiskers (0.2 s travel time) (Fig. 1a) for 1 s, after which it was retracted (0.2 s retraction time). The sample epoch (1.3 s total) was the time from onset of pole movement to 0.1 s after the pole started to retract (Fig. 1a). The delay epoch lasted for another 1.2 s after completion of pole retraction (1.3 s or 1.2 s total). An auditory 'go' cue separated the delay and the response epochs (pure tone, 3.4 kHz, 0.1 s). Licking early during the trial ('lick early' trials) was punished by an 'alarm' sound (siren buzzer, 0.05 s duration), followed by a timeout (1–1.2 s). After the go cue licking the correct lickport produced a water reward (approximately 3 μl); licking the incorrect lickport triggered a timeout (0–5 s). Trials in which mice did not lick within 1.5 s after the go cue (no response trials) were rare and typically occurred at the end of behavioural sessions. These no response and lick early trials were excluded from analyses (Figs 1–6).

Virus and tracer injection. The ALM (AP 2.5 mm, ML 1.5 mm, diameter 1.5 mm) is the cortical area that produced behavioural effects with photoinhibition during the delay epoch[3,24]. For the thalamic reticular nucleus the coordinates were AP −0.7, ML 1.6, DV 3.7 − 3.3 mm, as retrograde labelling from the $thal_{ALM}$ showed labelling in this sector of the thalamic reticular nucleus (Extended Data Fig. 9). Virus and tracer were injected through the thinned skull using a volumetric injection system (modified from Mo-10 Narishige)[48]. Glass pipettes (Drummond) were pulled and bevelled to a sharp tip (outer diameter around 20–30 μm), back-filled with mineral oil and front-loaded with viral suspension immediately before injection. The injection rate was 15 nl per min. See Supplementary Table 2 for description of viruses and injection coordinates used for each experiment. We used the following viruses and tracers: AAV2/1-CAG-EGFP (Penn vector Core, University of Pennsylvania), AAV2/10 CAG-flex-ChR2(H134R)-tdTomato (Penn vector Core, University of Pennsylvania), AAV1-CAG-mRuby2-Flag[49], wheat germ agglutinin (WGA)–Alexa Fluor 555 (Thermo Fisher Scientific)[50] (WGA–Alexa555) and Red RetroBeads (Lumafluor).

Histology. For anterograde and retrograde anatomy[27,51] (Extended Data Figs 1, 8, 9) mice were perfused transcardially with PBS followed by 4% PFA/0.1 M PB. The brains were fixed overnight and transferred to 20% sucrose before sectioning on a freezing microtome. Coronal, 50-μm free-floating sections were processed using standard fluorescent immunohistochemical techniques. All sections were stained with NeuroTrace 435/455 Blue Fluorescent Nissl stain (Thermo Fisher Scientific, N21479). Slide-mounted sections were imaged on a Zeiss microscope with a Ludl motorized stage controlled with Neurolucida software (MBF Bioscience). Imaging was done with a 10× objective and a Hamamatsu Orca Flash 4 camera. Each coronal section was made up of 80–200 tiles merged with Neurolucida software.

To reconstruct recording and photostimulation locations (Extended Data Figs 2, 4), mice were perfused transcardially with PBS followed by 4% PFA/0.1 M PB. The brains were fixed overnight and sectioned on a microtome at 100 μm thickness. Images were acquired on a macroscope (Olympus MVX10). Electrode tracks labelled with DiI were used to determine the recording locations. Tissue damage caused by optical fibres was used to determine photoinhibition locations.

For cell counting (Extended Data Fig. 1d), neurons labelled with WGA–Alexa555 were detected using Neurolucida software (MBF Bioscience). The whole brain image stack was registered to the Allen Institute Common Coordinate Framework (CCF) of the mouse brain using a MATLAB-based script (Mike Economo, Janelia Farms). The coordinates of detected WGA–Alexa555 labelled neurons were counted in the brain structures annotated in the Allen reference atlas.

We used Fluorender[52] to create 3D-reconstructed images of anterograde and retrograde signals (Extended Data Fig. 1e). GFP signals and densities of retrogradely labelled cells were overlaid. Cell densities were based on the cell counts described above. For individual retrogradely labelled neurons, the number of other surrounding retrogradely labelled neurons within the ± 100-μm cube were counted to estimate cell density.

Muscimol infusion. Cannulas (26GA, PlasticsOne) were implanted bilaterally near the VM/VAL and control locations (Extended Data Fig. 3; cannula coordinates in Supplementary Table 1). An injection needle was inserted into the guiding cannula, projecting 1.7 mm beyond the cannula tip. Muscimol·HBr (3–100 ng, Sigma-Aldrich) dissolved in 50 nl cortex buffer (125 mM NaCl, 5 mM KCl, 10 mM glucose, 10 mM HEPES, 2 mM $MgSO_4$, 2 mM $CaCl_2$, pH adjusted to 7.4) was injected through the volumetric injection system. The control solution was cortex buffer without muscimol.

Control behaviour was paused after mice performed 120–200 trials in a session and muscimol was infused for 4.5 ± 0.7 min (mean ± s.d., $n = 50$), after which behaviour resumed. As the infusion step requires pausing behaviour, which by itself can increase behavioural variability, identical procedures were also performed without infusion. After the last session of muscimol infusion, fluorescent muscimol bodipy (100 ng in 100 nl DMSO) was infused and mice were perfused immediately. Fluorescence and tissue damage caused by the injection needle were used to identify muscimol infusion locations. Each muscimol concentration was tested once per injection site.

For muscimol infusions near the VM/VAL, the ipsilateral bias lasted for the whole session (Extended Data Fig. 3b). After mice were released from head-fixation, ipsilateral circling was scored in the home cage. With the small dose of muscimol tested (1.8–5.9 ng), we did not observe circling (data not shown)[53].

Photoinhibition. Supplementary Table 1 provides coordinates and photostimulus powers for each experiment. Photoinhibition was used in 25% (Figs 1, 3a–f, 6) or 25–50% (Figs 3g, 4) of the behavioural trials. To prevent mice from distinguishing photoinhibition trials from control trials using visual cues, a 'masking flash' (forty 1 ms pulses at 10 Hz) was delivered using 470 nm LEDs (Luxeon Star) near the eyes of the mice throughout the trial. Trimming whiskers prevents mice from performing this task[3].

Photostimuli from a 473 nm laser (Laser Quantum) were controlled by an acousto-optical modulator (AOM; Quanta Tech) and a shutter (Vincent Associates). Photoinhibition of the ALM was performed through the clear-skull cap (beam diameter at the skull: 400 μm at 4σ). We stimulated parvalbumin-positive interneurons in PV-IRES-Cre mice crossed with Ai32-reporter mice expressing ChR2 (Figs 1, 6 and Extended Data Figs 8, 10). Behavioural and electrophysiological experiments showed that photoinihibition in the PV-IRES-Cre × Ai32 mice was indistinguishable from the VGAT–ChR2–EYFP mice (data not shown)[3].

To silence the cortex during the delay epoch (Figs 1, 6 and Extended Data Figs 8, 10), we photostimulated for 1.3 s, including the 100 ms ramp, starting at the beginning of the epoch. Photoinhibition silences a cortical area of 1 mm radius (at half-maximum) through all cortical layers. We used 40 Hz photostimulation with a sinusoidal temporal profile (1.5 mW average power) and a 100-ms linear ramp during the laser offset (this reduced rebound neuronal activity)[3]. The light transmission through the intact skull is 50%[3]. See Supplementary Table 1 for the animals, coordinates and power used for each experiment.

To silence the thalamus, the photostimuli were delivered through a 200-μm diameter optical fibre (Thorlabs). We used a continuous photostimulus with a 100-ms linear ramp at the offset (Figs 1d, 3–5). The photostimulus was applied for 1.2–1.3 s, including the 100-ms ramp, starting at the beginning of the delay epoch and terminating at the end of the delay epoch. Photoinhibition reduced activity (0.5–1.1 mm from the tip of the optical fibre) to 15.9 ± 9.3% (mean ± s.e.m., Extended Data Fig. 2d).

On the basis of retrograde labelling (Extended Data Fig. 1), we silenced at least 16,558 ALM-projecting thalamic neurons. For M1 silencing, we silenced at least 26,599 ALM-projecting neurons within a 1 mm radius from the laser centre. In the contralateral ALM we silenced at least 38,062 neurons projecting to the recorded side of the ALM (Extended Data Fig. 1d).

To silence the thalamus for behavioural experiments (Fig. 1) and current injection experiments (Extended Data Fig. 5), we avoided stimulating any uncharacterized

GABAergic projection neurons. We expressed ChR2 selectively in the TRN, by injecting AAV2/10 CAG-flex-ChR2(H134R)-tdTomato into TRN of Gad2-IRES-Cre mice. We implanted an optical fibre over the VM/VAL, but other thalamic nuclei projecting to the ALM were also likely to have been affected (Extended Data Fig. 2).

Extracellular electrophysiology. Recordings were made from the left hemisphere. Recording locations were deduced from electrode tracks (see 'Histology' and Extended Data Fig. 4). For ALM recordings, a small craniotomy (1 mm diameter) was made one day before the recording session[3]. Extracellular spikes were recorded using NeuroNexus silicon probes (A4x8-5 mm-100-200-177) or Janelia silicon probes (A2x32-8 mm-25-250-165). The 32- or 64-channel voltage signals were multiplexed, recorded on a PCI6133 board at 312.5 kHz or 400 kHz (National Instrument), and digitized at 14-bits. The signals were demultiplexed into the 32- or 64-voltage traces, sampled at 19,531.25 or 25,000 Hz, respectively, and stored for offline analyses. 3–5 recording sessions were obtained per craniotomy. Recording depth was inferred from manipulator readings and verified based on histology[3]. The craniotomy was filled with cortex buffer and the brain was not covered. The tissue was allowed to settle for at least 10 min before the recording started.

For VM/VAL recordings, a small craniotomy was made over the dorsal medial somatosensory cortex (centre, bregma AP −1.5 mm, ML 1.8 mm). For optrode recording from the VM/VAL, we used NeuroNexus silicon optrodes (A4x8-5 mm-100-400-177 with a 105-μm diameter optical fibre placed 200 μm above recording sites on the inner right shank). For SNr recordings, a small craniotomy was made over the visual area (centre, bregma AP −3.5 mm, ML 3 mm). Electrodes were driven down about 4.5 mm to reach SNr. RetroBeads injected near the VM/VAL labelled SNr extensively in the caudal–rostral and medial–lateral directions[54] (Extended Data Fig. 9). Our recording probes (spanning ML 600 μm) sampled a large region of the SNr (medial, lateral, rostral and caudal). The effects of ALM photoinhibition on SNr activity did not vary spatially and the data were pooled.

***In vivo* whole-cell recording (also see Supplementary Information).** Whole-cell recordings were made using pulled borosilicate glass (Sutter instrument)[55]. A small craniotomy (100–300 μm diameter) was created over the ALM or M1 (bregma AP 0.0 mm, ML 2.0 mm) under isofluorane anaesthesia and covered with cortex buffer during recording. Whole-cell patch pipettes (7–9 MΩ) were filled with internal solution (in mM): 135 K-gluconate, 4 KCl, 10 HEPES, 0.5 EGTA, 10 Na_2-phosphocreatine, 4 Mg-ATP, 0.4 Na_2-GTP and 0.3% Biocytin (293–303 mOsm, pH 7.3). The V_m was amplified (Multiclamp 700B, Molecular Devices) and sampled at 20 kHz using WaveSurfer (http://wavesurfer.janelia.org/). V_m were not corrected for liquid junction potential. After the recording the craniotomy was covered with Kwik-Cast (World Precision Instruments). Each animal was used for 2–3 recording sessions. Recordings were made from 350 to 850 μm below the pia. Neuronal responses to thalamic or cortical inactivation were similar across depths and were pooled for analysis.

To obtain mean V_m dynamics of each neuron (Figs 3g, 4 and Extended Data Figs 5, 6), we clipped off action potentials. We found the point in the V_m where the derivative passed 3 s.d. from the baseline (kink). Baseline and s.d. were calculated from 2.5 ms to 1.5 ms before the spike peak. Points from −0.5 to 5 ms around the kink were interpolated. The s.e.m. of the V_m was estimated by bootstrapping. The action-potential threshold was defined as the difference between baseline V_m (0–0.5 s before onset of each behavioural trial) and the spike threshold. Whole-cell recordings with more than 20 behavioural trials were pooled to calculate action-potential thresholds and membrane time constants ($n = 60$).

The onset of the V_m change after photoinhibition (Fig. 3g and Extended Data Fig. 6b, e, f) was the time when the V_m changed by more than 3 s.d. from the baseline. The baseline and s.d. were calculated from 20 ms before the photostimulus onset until 2 ms after onset of the photostimulation trials. A similar procedure was used to estimate the onset of V_m change after thalamus photoactivation (Extended Data Fig. 6c). The s.e.m. of the onsets was determined by bootstrapping.

Behavioural data analysis. Behavioural performance was the fraction of correct trials, excluding lick early and no response trials. We separately computed the performance for contra and ipsi trials relative to the manipulation side (Fig. 1 and Extended Data Fig. 3). Behavioural effects of photoinhibition were quantified by comparing the performance with photoinhibition with control performance (Fig. 1c, d). Significance of the performance change was determined using Student's *t*-test. Photoinhibition of the ALM or thalamus caused only small changes in lick early rates, no response rates and licking latency (Supplementary Information).

The performance change due to muscimol silencing was computed as the fraction of correct trials after infusion (the 100 trials immediately after muscimol infusion) relative to the fraction of correct trials before muscimol infusion (the 100 trials right before muscimol infusion). Performance change in the muscimol condition was compared with that during the control condition. Significance was determined using Student's *t*-test (Extended Data Fig. 3). Muscimol infusion did not increase the lick early rates ($P > 0.1$; paired *t*-test) and slightly increased the no response rate from 0 to 1% (that is, from no no response trial to one no response trial in a session, $P = 0.02$).

Electrophysiology data analysis. Detailed spike sorting procedures have been described[3]. Recording depths were estimated from histology[3] (Extended Data Fig. 4). The extracellular recording traces were band-pass filtered (300 Hz–6 kHz). Events that exceeded an amplitude threshold (4 s.d. of the background) were subjected to manual spike sorting to extract single units. For the low thalamus inactivation experiments (Fig. 5), spikes were sorted using JRclust (program by J. Jaeyoon Jun, APIG, Janelia Farm). Spikes were binned by 1 ms and averaged over 200 ms (Figs 2, 3, 5, 6).

In the ALM, 1,214 single units were recorded across 57 behavioural sessions. Spike widths were computed as the trough-to-peak interval in the mean spike waveform. The distribution of spike widths was bimodal (Extended Data Fig. 4); units with width <0.4 ms were defined as putative fast-spiking neurons (166 out of 1,214) and units with width >0.6 ms as putative pyramidal neurons (1,006 out of 1,214). This classification was previously verified by optogenetic tagging of GABAergic neurons[3]. Units with intermediate spike widths (0.4–0.6 ms, 42 out of 1,214) were excluded from our analyses. We concentrated our analyses of the ALM on putative pyramidal neurons (Figs 2, 3, 5).

In the thalamus, 790 single units were recorded across 73 behavioural sessions. Unit locations were determined from the locations of the relevant recording sites, which in turn were reconstructed from histology (Extended Data Fig. 4). All units were recorded in a narrow range of AP locations (between bregma −1 mm and −2 mm). We therefore overlaid units on one coronal section for spatial analysis (bregma −1.76, Fig. 6d). Neurons in the VM/VAL are excitatory. The distribution of spike widths was unimodal with a tail with short spike widths; this suggests that some units corresponded to GABAergic axons from the TRN or SNr[56]. Units with spike width >0.5 ms were selected as putative thalamic neurons (672 out of 790) and we concentrated our analyses on these neurons. However, our conclusions (Figs 2, 6) are valid if all the units were pooled. To select units in the VM/VAL we applied a stringent spatial criterion; units within 0.4 mm from the VM/VAL centre (determined from retrograde labelling experiments, Extended Data Fig. 1) were scored as VM/VAL neurons (313 out of 790). This criterion could be relaxed to 1.0 mm from the VM/VAL centre without changing our conclusions, as neurons within 1.0 mm from the VM/VAL centre showed robust inhibition (to 36% of control activity during the first 100 ms inhibition, also see Extended Data. Fig. 8b). Furthermore, randomly jittering neuron locations by 200 μm in the AP, ML and DV directions did not affect our conclusions.

In the SNr, 227 single units were recorded across 23 behavioural sessions. SNr GABAergic neurons have narrower spike widths than dopaminergic neurons in the nearby substantia nigra pars compacta[57]. Units with spike trough-to-peak width <0.45 ms were selected as putative GABAergic neurons (spike width at half maximum, 0.143 ± 0.030 ms (mean ± s.d.), 181 out of 227). These units have high spike rates (40.9 ± 21.5 (mean ± s.d.), $n = 181$). For comparison, neurons with longer spike widths have lower spikes rates (23.4 ± 17.0 (mean ± s.d.), $n = 46$). We concentrated our analyses on putative GABAergic neurons. We used bootstrapping to test whether there were more neurons significantly down-modulated than up-modulated. The null hypothesis was that there were equal or more up-modulated neurons. In each round of bootstrapping, we replaced the original neurons with a re-sampled dataset. The number of down-modulated and up-modulated neurons were counted and compared. The *P* value was the fraction of times the bootstrapping produced a consistent result as the null hypothesis.

Neurons were tested for trial-type selectivity during the sample, delay or response epochs by comparing spike counts during contra and ipsi trials (*t*-test, $P < 0.05$; Fig. 2 and Extended Data Fig. 10). Neurons that significantly differentiated trial types during any one of the trial epochs were deemed as selective (704 out of 1,006 in the ALM, 204 out of 295 in the VM/VAL, 152 out of 181 in the SNr). Neurons with selectivity during the sample or delay epochs were classified as having preparatory activity. Neurons with significant selectivity during the response epoch were classified as having peri-movement selectivity. Selective neurons were classified as contra-preferring or ipsi-preferring on the basis of their total spike counts across all three trial epochs[27] (Fig. 2 and Extended Data Fig. 10). To compute contra-selectivity, we took the firing rate difference between the contra trials and ipsi trials for each neuron. The ipsi-selectivity was computed similarly. Only trials in which mice correctly reported pole locations were included to compute selectivity.

For the peri-stimulus time histograms (PSTHs; Figs 3, 5, 6 (except the top panels in Figs 3b, 6b) and Extended Data Fig. 7), correct and incorrect trials were included, as photoinhibition reduced neural activity irrespective of the response outcomes. To analyse the effects of photoinhibition, units with at least 5 (Fig. 3,

$n = 314$; Fig. 6, $n = 201$) or 25 (Fig. 5, $n = 160$) photoinhibition trials were selected. Bootstrapping was used to estimate s.e.m. (Figs 3, 6 and Extended Data Figs 2, 7, 8, 10). As the effect of photoinhibition began 10–20 ms after photostimulus, we used 20–120 ms after photostimulus onset to measure the amplitude of inactivation (Figs 3, 6 and Extended Data Fig. 10). For Figs 3c, 5b, 6c (top), both contra and ipsi trials were pooled to calculate mean spike rate. For Fig. 5c, neurons with spike rates higher than two spikes per second during both control and photoinhibition conditions were included ($n = 73$).

The onset of inactivation was defined as the time when the V_m passed 3 s.d. of the control condition. The s.d. was calculated using the control condition during the delay epoch. Changing the duration used to calculate the s.d. did not change the estimate of onset latency. We also detected the onset by comparing the PSTHs during the photoinhibition and control conditions using a Student's t-test, with consistent results. To estimate the s.e.m. of the inhibition onset, we randomly sampled neurons with replacement and used the bootstrapped dataset to compute the onset of photoinhibition. This procedure was repeated 1,000 times.

Statistics. The sample sizes are similar to sample sizes used in the field (more than 100 units per brain region). No statistical methods were used to determine sample size. We did not exclude any animal for data analysis. Trial types were randomly determined by a computer program. During spike sorting, experimenters cannot tell the trial type, so experimenters were blind to conditions. All comparisons using t-tests are two-sided. For the behavioural test of thalamus inhibition (Fig. 1), the data points are normally distributed (tested using Kolmogorov–Smirnov test). All bootstrapping was done over 1,000 or 10,000 iterations.

Data availability. Datasets will be shared at https://crcns.org/ in the NWB format[58] (https://dx.doi.org/10.6080/K03F4MH2). All other data that support the findings of this study are available from the corresponding author upon reasonable request.

45. Hippenmeyer, S. *et al.* A developmental switch in the response of DRG neurons to ETS transcription factor signaling. *PLoS Biol.* **3,** e159 (2005).
46. Madisen, L. *et al.* A toolbox of Cre-dependent optogenetic transgenic mice for light-induced activation and silencing. *Nat. Neurosci.* **15,** 793–802 (2012).
47. Vue, T. Y. *et al.* Sonic hedgehog signaling controls thalamic progenitor identity and nuclei specification in mice. *J. Neurosci.* **29,** 4484–4497 (2009).
48. Petreanu, L., Mao, T., Sternson, S. M. & Svoboda, K. The subcellular organization of neocortical excitatory connections. *Nature* **457,** 1142–1145 (2009).
49. Viswanathan, S. *et al.* High-performance probes for light and electron microscopy. *Nat. Methods* **12,** 568–576 (2015).
50. Tsuriel, S., Gudes, S., Draft, R. W., Binshtok, A. M. & Lichtman, J. W. Multispectral labeling technique to map many neighboring axonal projections in the same tissue. *Nat. Methods* **12,** 547–552 (2015).
51. Gerfen, C. R., Paletzki, R. & Heintz, N. GENSAT BAC Cre-recombinase driver lines to study the functional organization of cerebral cortical and basal ganglia circuits. *Neuron* **80,** 1368–1383 (2013).
52. Wan, Y., Otsuna, H., Chien, C. B. & Hansen, C. An interactive visualization tool for multi-channel confocal microscopy data in neurobiology research. *IEEE Trans. Vis. Comput. Graph.* **15,** 1489–1496 (2009).
53. Di Chiara, G., Morelli, M., Porceddu, M. L. & Gessa, G. L. Role of thalamic gamma-aminobutyrate in motor functions: catalepsy and ipsiversive turning after intrathalamic muscimol. *Neuroscience* **4,** 1453–1465 (1979).
54. Gulcebi, M. I. *et al.* Topographical connections of the substantia nigra pars reticulata to higher-order thalamic nuclei in the rat. *Brain Res. Bull.* **87,** 312–318 (2012).
55. Margrie, T. W., Brecht, M. & Sakmann, B. *In vivo*, low-resistance, whole-cell recordings from neurons in the anaesthetized and awake mammalian brain. *Pflugers Arch.* **444,** 491–498 (2002).
56. Barthó, P. *et al.* Ongoing network state controls the length of sleep spindles via inhibitory activity. *Neuron* **82,** 1367–1379 (2014).
57. Rossi, M. A., Fan, D., Barter, J. W. & Yin, H. H. Bidirectional modulation of substantia nigra activity by motivational state. *PLoS One* **8,** e71598 (2013).
58. Teeters, J. L. *et al.* Neurodata without borders: creating a common data format for neurophysiology. *Neuron* **88,** 629–634 (2015).
59. Chen, J. & Kriegstein, A. R. A GABAergic projection from the zona incerta to cortex promotes cortical neuron development. *Science* **350,** 554–558 (2015).
60. Shepherd, G. M. Corticostriatal connectivity and its role in disease. *Nat. Rev. Neurosci.* **14,** 278–291 (2013).

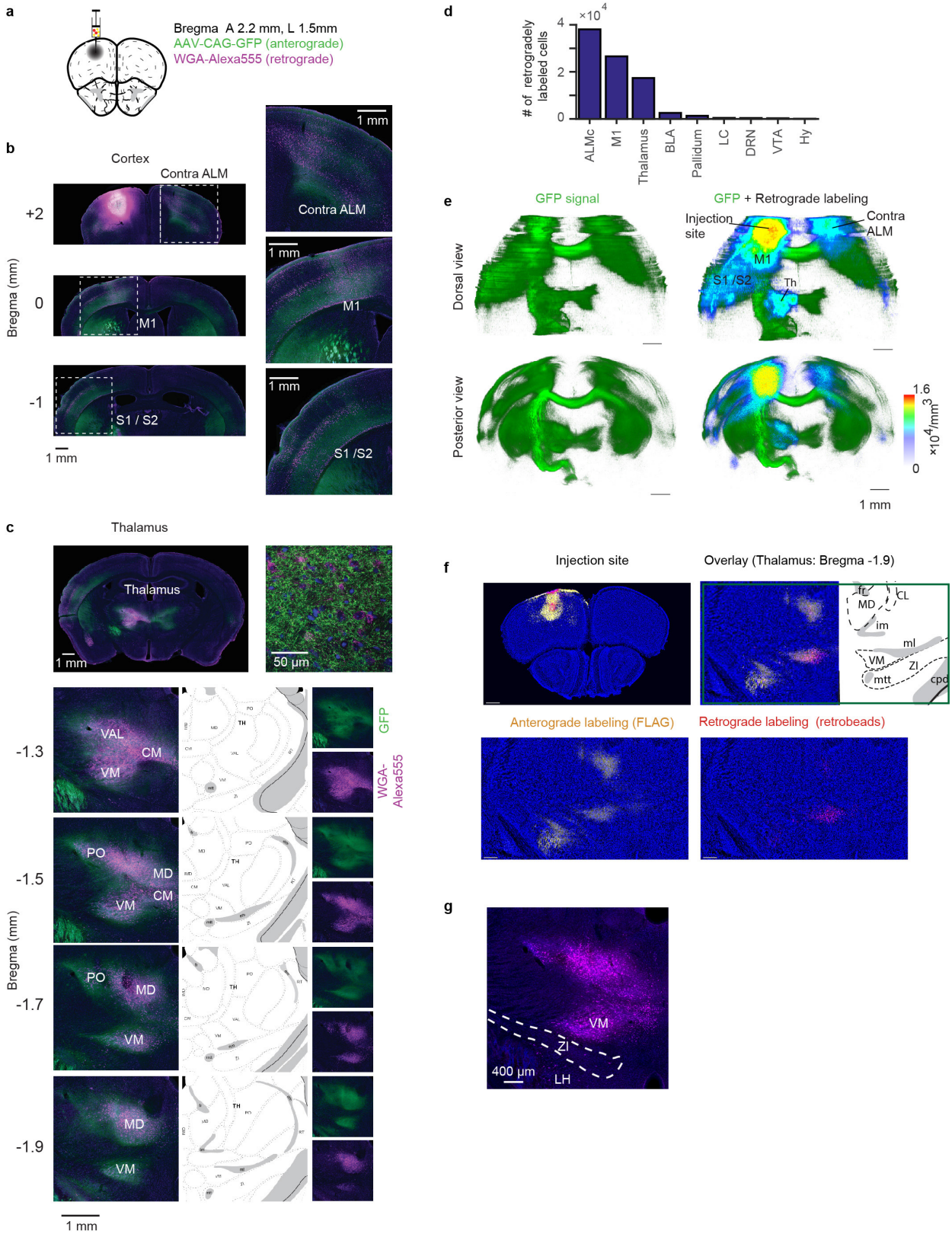

Extended Data Figure 1 | See next page for caption.

Extended Data Figure 1 | The ALM makes reciprocal connections with multiple cortical and thalamic areas. a, Co-injection of the anterograde tracer (AAV2/1-CAG-GFP) and retrograde tracer (WGA–Alexa555)[50]. **b**, Retrograde and anterograde labelling in the contralateral ALM, ipsilateral M1 and ipsilateral somatosensory cortex (S1/S2). Dashed boxes indicate magnified images on the right. Green, anterograde label (GFP); magenta, retrograde label (WGA–Alexa555); blue, Nissl stain. **c**, Thalamus (as in **b**). Anterograde labelling in the ipsilateral thalamus (with a weak contralateral projection); retrograde labelling was limited to the ipsilateral thalamus (top left). Confocal image of the thalamus (top right). Four coronal sections of ipsilateral thalamus (bottom left) and corresponding Allen Reference Atlas sections (http://mouse.brain-map.org/static/atlas) (bottom middle). Separate anterograde and retrograde label (bottom right). CM, centromedian nucleus of the thalamus; em, external medullary lamina of the thalamus; fr, fasciculus retroflexus; im, internal medullary lamina of the thalamus; IMD, intermediodorsal nucleus of the thalamus; MD, medial dorsal nucleus of the thalamus; ml, medial lemniscus; mtt, mammillothalamic tract; PO, posterior nucleus of the thalamus; RT; thalamic reticular nucleus, ZI, zona incerta. **d**, Number of neurons labelled by retrograde injection into the left ALM in cortical and subcortical areas. 38,062 (contra ALM); 26,599 (M1); 17,375 (thalamus); 2,532 (basolateral amygdala(BLA)); 1,312 (pallidum and basal forebrain); 427 (locus coeruleus (LC)); 377 (dorsal raphe nucleus (DRN)); 263 (ventral tegmental area (VTA)); and 59 (hypothalamus (HY)). For cortical areas we limit the neuron counting to the regions manipulated in the photoinhibition experiments (Fig. 4 and Methods). In subcortical areas we counted all neurons. **e**, 3D reconstruction. Left, anterograde GFP signal. Right, anterograde GFP signal (green) overlaid with heatmap representing density of retrogradely labelled neurons. **f**, Additional experiments using anterograde (AAV2/1-CAG-Flag) and retrograde (RetroBeads) tracers (Methods). Left, injection in the ALM. Retrograde labelling (red) is spatially restricted to the centre of the ALM (with some spreading to layer (L)1 and the pia). The three other panels show the thalamus. **g**, Retrograde tracer injection in ALM only rarely labelled zona incerta neurons (total count, 31 ± 2 per brain); none of these were positive for somatostatin (a marker for cortex projecting GABAergic zona incerta neurons, data not shown)[59]. This excludes the possibility that zona incerta GABAergic neurons directly inhibit the ALM during optogenetic manipulation of the thalamus.

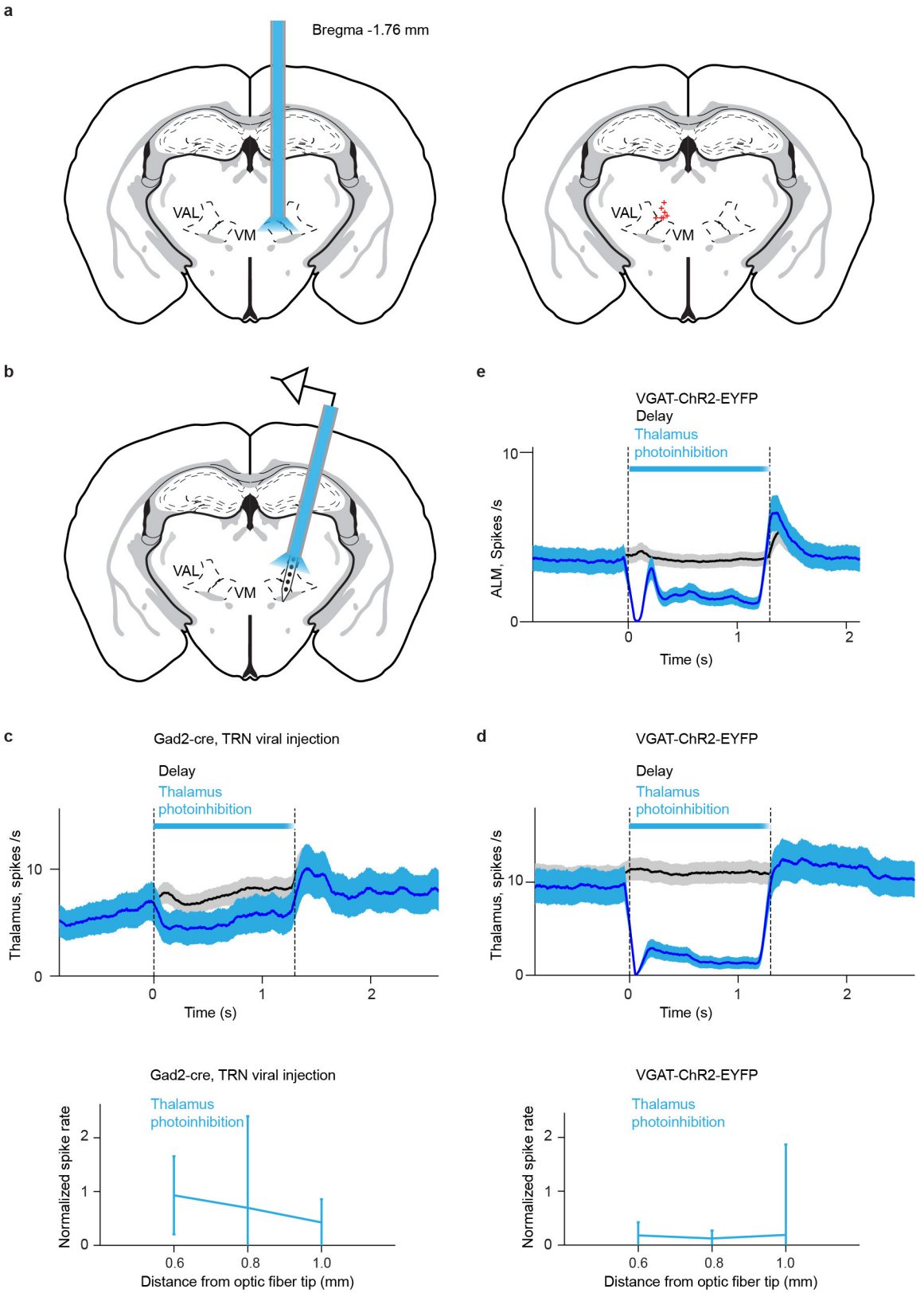

Extended Data Figure 2 | See next page for caption.

Extended Data Figure 2 | Optical fibre locations and thalamus photoinhibition. a, Left, schematic of thalamus photoinhibition through an optical fibre. Right, optical fibre locations were overlaid on a coronal section of the Allen Reference Atlas ($n = 7$ mice). **b**, Schematic of thalamus recording during photoinhibition using an optrode. **c**, Top, PSTH of putative thalamic neurons recorded by an optrode during control (black) and photoinhibition (blue) conditions in Gad2-IRES-Cre mice. Virus expressing ChR2 in a Cre-dependent manner was injected in the VM/VAL projection zone of TRN. The magnitude of photoinhibition depends on the overlap of light intensity and axonal ChR2 expression. The fibre optic was 1 mm dorsal of the VM/VAL, which probably explains why the photoinhibition was stronger 1 mm from the fibre than closer to the fibre output. Averaging window, 100 ms. Bottom, normalized spike rate (mean spike rate during photoinhibition divided by mean spike rate during control) versus distance from the optical fibre. Error bars indicate s.d. $n = 26, 41, 17$ cells at a distance of 0.6, 0.8, 1.0 mm, respectively. Laser power at the tip of optical fibre, 10 mW. **d**, Top, PSTH of thalamic neurons recorded by an optrode during control (black) and photoinhibition (blue) conditions in VGAT–ChR2–EYFP mice. Averaging window, 100 ms. Bottom, normalized spike rate (mean spike rate during photoinhibition divided by mean spike rate during control) versus distance from optical fibre. Error bars indicate s.d. $n = 34, 42, 38$ cells; at a distances of 0.6, 0.8, 1.0 mm, respectively. Silencing extended beyond the VM/VAL and included other thalamic nuclei that project to ALM and nearby cortical areas. Silencing using VGAT–ChR2–EYFP (**d**) was more potent than with Gad2-IRES-Cre mice (**c**). Laser power at the tip of optical fibre, 10 mW. **e**, PSTH of ALM neurons during control (black) and thalamus photoinhibition (blue) conditions. Laser power at the tip of optical fibre 10 mW, $n = 314$ cells. Averaging window, 100 ms.

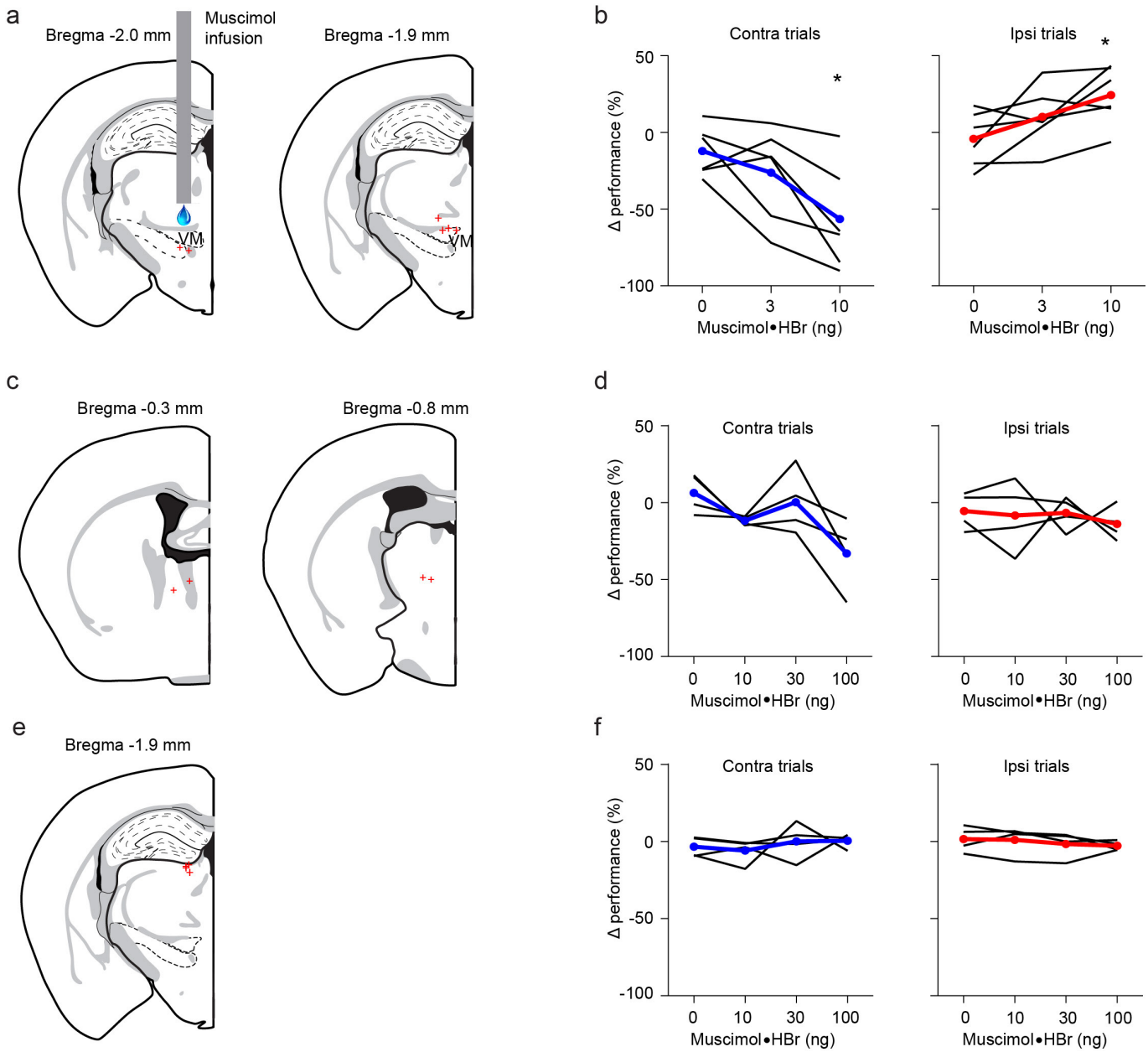

Extended Data Figure 3 | Effects of thalamic muscimol infusions on behaviour. a, Muscimol infusion locations (red crosses) near the VM/VAL. Sites from left ($n = 3$) and right ($n = 3$) hemispheres were mapped onto the left hemisphere. **b**, Small amounts of muscimol (1.5–5 ng) infused near the VM/VAL produced ipsilateral bias. Left, performance change in contra trials after muscimol infusion. Right, performance change in ipsi-trials after muscimol infusion. Each line represents an infusion site ($n = 6$, same mice as in **a**). *$P < 0.05$, paired t-test. **c**, Muscimol infusion locations in the anterior part of the thalamus (red crosses). Sites from left ($n = 2$) and right ($n = 2$) hemispheres were mapped onto the left hemisphere. **d**, Muscimol infusions in the anterior part of the thalamus (around 1.1–1.6 mm anterior to the centre of VM/VAL; same mice as in **c**). Note that much higher muscimol concentrations (10 times of those used near the VM/VAL), did not affect behaviour. **e**, Muscimol infusion locations in the dorsal part of the thalamus (red crosses). Sites from left ($n = 2$) and right ($n = 2$) hemispheres were mapped onto the left hemisphere. **f**, Muscimol infusions in the dorsal part of the thalamus (around 0.2–0.5 mm dorsal to medial dorsal thalamus, same mice as in **e**). Note that much higher muscimol concentrations (10 times of those used near the VM/VAL), did not affect behaviour.

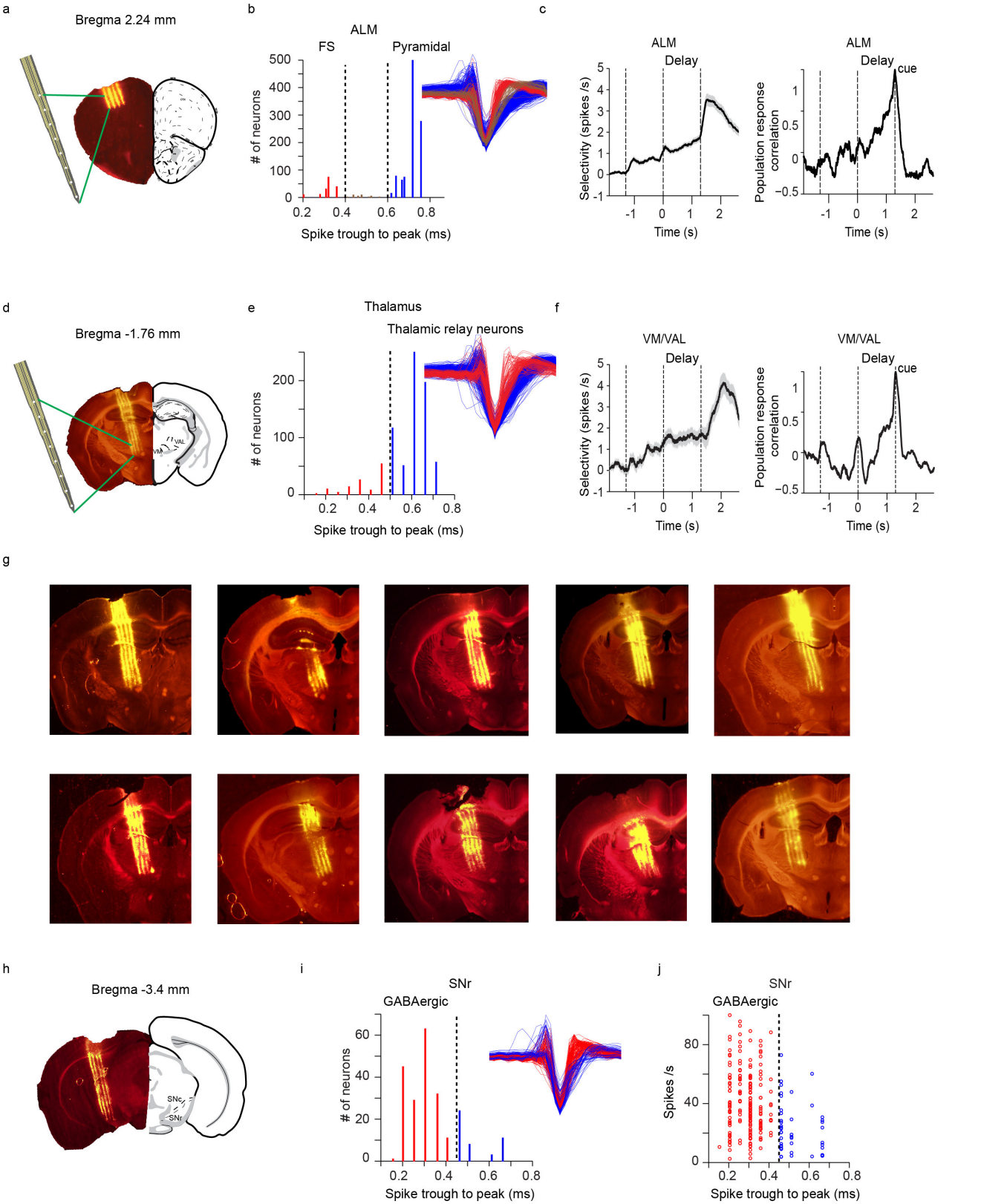

Extended Data Figure 4 | See next page for caption.

Extended Data Figure 4 | Recording sites and neuron types recorded in the ALM, thalamus and SNr. a, Example electrode tracks in ALM labelled with DiI. **b**, Single-unit classification in the ALM. Left, putative fast-spiking (FS) interneurons (red, $n = 166$) and putative pyramidal neurons (blue, $n = 1{,}006$) were separated on the basis of the histogram of spike widths[3] (Methods). A small subset of neurons with intermediate spike durations were not classified (brown, $n = 42$). Right, mean spike waveform of each unit. **c**, Left, average population selectivity in spike rate of ALM neurons. To compute population selectivity, we first determined each neuron's preferred trial type using spike counts from half of the trials; selectivity was calculated as the spike rate difference between the preferred and non-preferred trial types for the other half of trials. The s.e.m. was estimated by bootstrapping over neurons. Averaging window, 200 ms. Right, population response correlation of ALM neurons. The smoothed response was mean subtracted and normalized to the variance during the entire trial epoch. The Pearson's correlation at a particular time was calculated between the population response vector at that time point and the population response vector at cue onset[27]. **d**, Example electrode tracks in the VM/VAL. **e**, Single-unit classification of neurons in thalamus. Left, putative thalamic neurons (blue, $n = 672$) were selected on the basis of the histogram of spike widths (Methods). Right, mean spike waveform of each unit. **f**, Average population selectivity in spike rate (left) and population correlation (right) of VM/VAL neurons. **g**, Additional electrode tracks in the thalamus ($n = 10$ mice). Electrode tracks were used to determine whether recorded neurons were in the VM/VAL. **h**, Example electrode tracks in the SNr. **i**, Single-unit classification in SNr. Left, putative GABAergic neurons (red, $n = 181$) were selected on the basis of the histogram of spike widths and their high spike rates (Methods). Right, mean spike waveform of each unit. **j**, Spike rate of single units in the SNr. Putative GABAergic neurons have a mean spike rate of 40.9 ± 21.5 (mean $\pm$ s.d., $n = 181$). The other neurons have a mean spike rate of 23.4 ± 17.0 (mean $\pm$ s.d., $n = 46$).

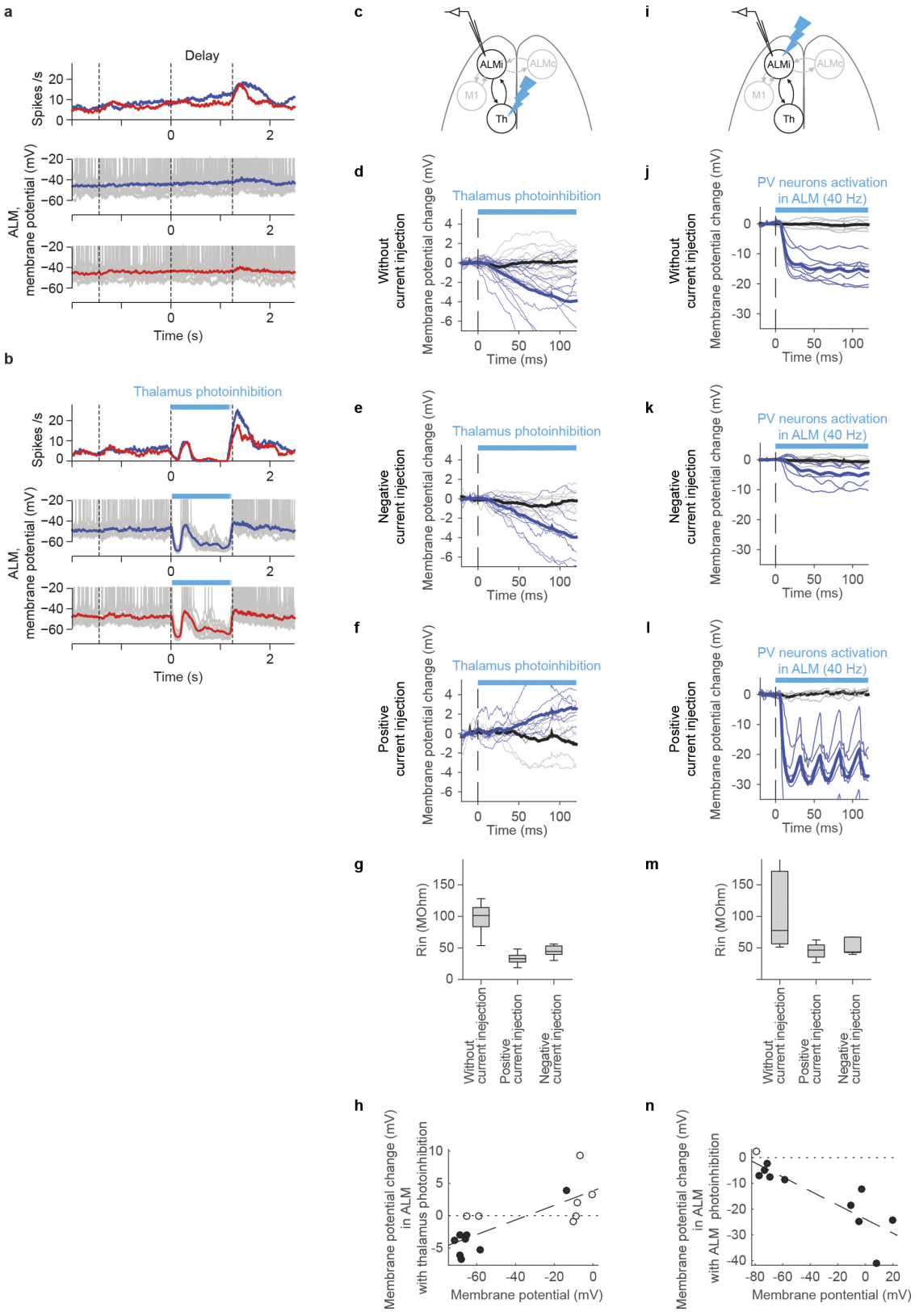

Extended Data Figure 5 | See next page for caption.

Extended Data Figure 5 | Hyperpolarization of ALM neurons during thalamus photoinhibition is caused by loss of excitation. a, **b**, ALM neuron during thalamus photoinhibition. Top, PSTH during control (**a**) and photoinhibition (**b**) trials. Bottom, V_m during each trial type (10 trials each). Red and blue lines, trial averaged V_m. **c**–**h**, V_m changes in ALM neurons after thalamus photoinhibition (non-behaving animals). In this experiment thalamic photoinhibition was low (Cre-dependent ChR2-AAV injected near the VM/VAL projection zone of the TRN in Gad2-IRES-Cre mice). Photoinhibition is much more potent in VGAT–ChR2 mice, because the vast majority of TRN and SNr neurons are $ChR2^+$. **c**, Schematic. **d**, V_m changes after light onset. Average control, black; average photoinhibition, blue; $n = 14$ cells. Thin lines, individual neurons. Consistent with data from behaving VGAT–ChR2 mice (Fig. 3g), we observed significant hyperpolarization after light onset. **e**, Same as **d** during negative current injection ($n = 9$ cells). V_m is near the reversal potential for inhibitory currents, and excitatory currents were amplified. **f**, Same as **d** during positive current injection ($n = 6$ cells). V_m is near the reversal potential for excitatory currents, and the inhibitory currents are amplified. **g**, Input resistance was similar during positive and negative current injections ($P = 0.05$, rank-sum test). **h**, Relationship between V_m in non-photoinhibition condition versus V_m changes with photoinhibition (ΔV_m). V_m and ΔV_m were calculated between 100–120 ms after the onset of light. We plotted data from positive and negative current injections, because the input resistances were similar (see **g**). Slope of linear regression (dashed line) is larger than zero ($P < 0.0001$, bootstrapped), indicating that hyperpolarization is mainly caused by loss of excitation. Black circles, cells with significant change of V_m. **i**–**n**, The time course of V_m change in ALM neurons during photoactivation of local $parvalbumin^+$ (PV^+) neurons expressing ChR2. This experiment shows that silencing by increased inhibition can be distinguished from loss of excitation with our method. Panels are as in **c**–**h**. **i**, Schematic. **j**, $n = 7$ cells. **k**, **l**, Hyperpolarization was reduced during negative current injection ($n = 5$ cells, **k**), and enhanced during positive current injection ($n = 5$ cells, **l**). **m**, Input resistances during positive and negative current injections were similar ($P = 0.662$, rank-sum test). **n**, The slope of linear regression is smaller than zero ($P < 0.0001$, bootstrapped), which indicates that hyperpolarization was mainly due to increased inhibition. Note that the effect of current injection is opposite from that of thalamic inactivation (compare with **h**).

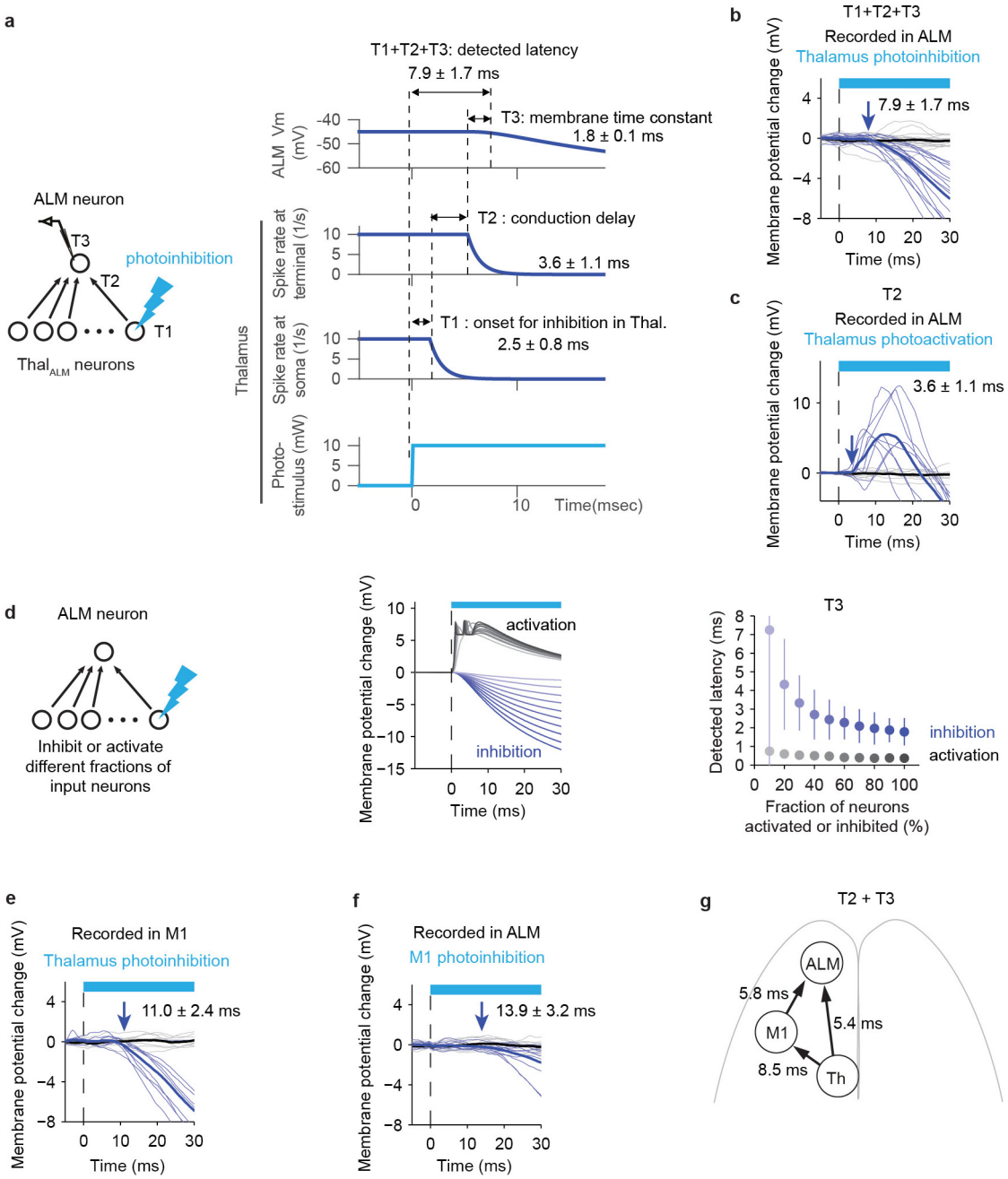

Extended Data Figure 6 | Onset of V_m changes after thalamic and cortical photoinhibition. a, Contributions to the time of detected V_m change in the ALM after photoinhibition of the thalamus. The time between photostimulus onset and silencing in thalamus is T1 = 2.5 ± 0.8 ms (Fig. 3f). The propagation delay from thalamus to the thalamic terminals in the ALM is T2 = 3.6 ms (see **c**). An additional T3 = 1.8 ms is required to hyperpolarize the V_m of ALM neurons, because of the synaptic and membrane time constants. T1 + T2 + T3 explains the measured latency (7.9 ± 1.7 ms). T2 + T3 is defined as the latency difference. **b**, The time course of V_m change in ALM neurons after thalamic photoinhibition (same as Fig. 3g). Other panels in this figure (**c**, **e**, **f**) follow the same format. **c**, The time course of V_m change in ALM neurons after thalamus photoactivation in non-behaving naive Olig3-Cre[47] × Ai32 mice (labelling the thalamus specifically, $n = 9$ cells). Since we used a high laser power intensity (10 mW), we assume spikes were generated in the thalamus within 1 ms. This time provides an estimate for the conduction delay of thalamocortical neurons (T2). **d**, Model-based estimation of the time required to depolarize (black) or hyperpolarize (blue) ALM neurons (T3). Left, schematic. Middle, mean V_m traces. Right, latency (mean ± s.e.m., $n = 300$ per condition). Conduction delay was set to zero. Traces or plots with a different colour indicate data with different fractions of activated/inhibited neurons: 10–100% (from lighter to darker). Even when all the input neurons were inhibited, we expect to observe a latency of 1.8 ± 0.7 ms (mean ± s.e.m.). See Supplementary Information for details. **e**, The time course of V_m change in M1 putative pyramidal neurons after thalamus photoinhibition during the delay epoch in behaving mice ($n = 9$ cells). As it takes 2.5 ± 0.8 ms to reduce spike rates in thal$_{ALM}$ after photostimulation onset, we estimate that it takes 8.5 ms for the thal$_{ALM}$ to affect M1 activity. **f**, The time course of V_m change in ALM neurons after M1 photoinhibition during the delay epoch in behaving mice ($n = 11$ cells). As it takes 8.1 ± 1.2 ms to silence the cortex (Fig. 6e), this implies it takes approximately 5.8 ms for changes in M1 activity to affect ALM activity. **g**, Summary of measured latencies. Time required to inhibit input structures is subtracted to show T2 + T3.

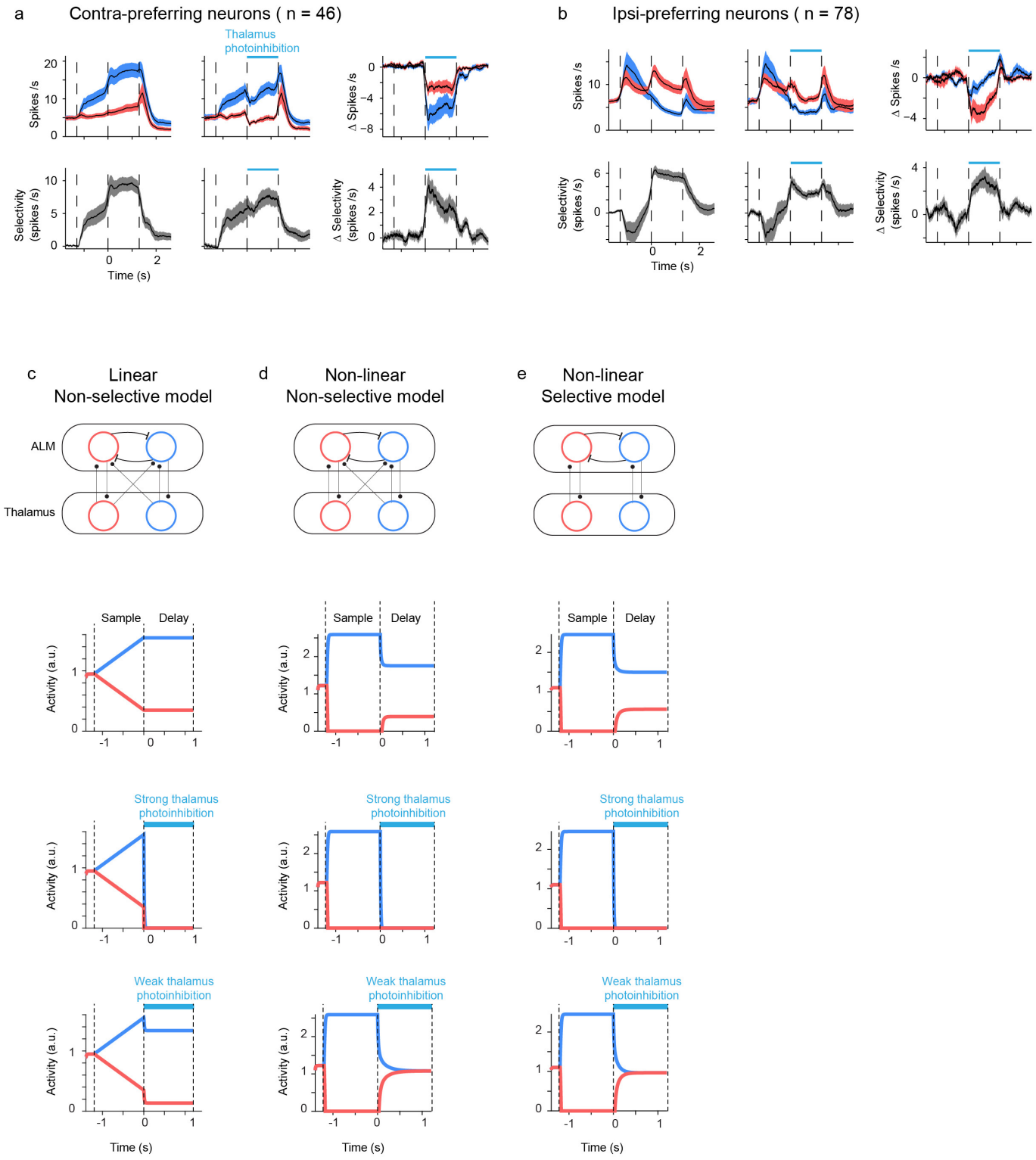

Extended Data Figure 7 | See next page for caption.

Extended Data Figure 7 | Effects of low thalamus inhibition on ALM selectivity and models of thalamo-ALM interactions. a, Average population PSTH (top left and middle) and population selectivity (bottom left and middle) of contra-preferring ALM neurons. Here, contra-preferring neurons are defined as neurons with significantly higher spike rates during the delay epoch of contra trials compared to ipsi trials (t-test, $P < 0.05$). We included neurons with spike rates higher than 2 spikes per s during both control and inactivation conditions. Selectivity was calculated as the spike rate difference between the contra and ipsi trial types. Averaging window, 200 ms. Average population PSTH (top middle) and selectivity (bottom middle) of contra-preferring ALM neurons during low thalamic photoinhibition. Average spike rate changes (top right) and average selectivity changes (bottom right) caused by low thalamic photoinhibition. The s.e.m. was estimated by bootstrapping over neurons. Blue, mean ± s.e.m. (bootstrap) of contra trials; red, mean ± s.e.m. of ipsi trials. **b**, The same plot as in **a** for ipsi-preferring neurons. **c**–**e**, We analysed model networks to better understand the possible interactions between the ALM and thalamus. Top, the models consist of two neurons (left- and right-preferring neurons, blue and red, respectively) in both the thalamus and ALM. Thalamus to ALM connections were either non-selective (**c**, **d**) or selective (**e**). Activity of the right (blue) and left (red)-preferring neurons during a lick right trial are plotted (second to fourth rows). Selective sensory input enters the ALM during the sample epoch, and selective activity is maintained during the delay epoch without sustained input (second row from the top). The models were tested in response to non-selective thalamic photoinhibition that was either high (third row) or low (fourth row). During high thalamus photoinhibition, activities of the right and left preferring neurons were reduced to zero in all models (consistent with Fig. 3). During low thalamus photoinhibition, selectivity was reduced to zero without large changes in mean spike rate in both nonlinear models (**d**, **e**) (consistent with Fig. 5), but not in a linear model (**c**). See Supplementary Information for details.

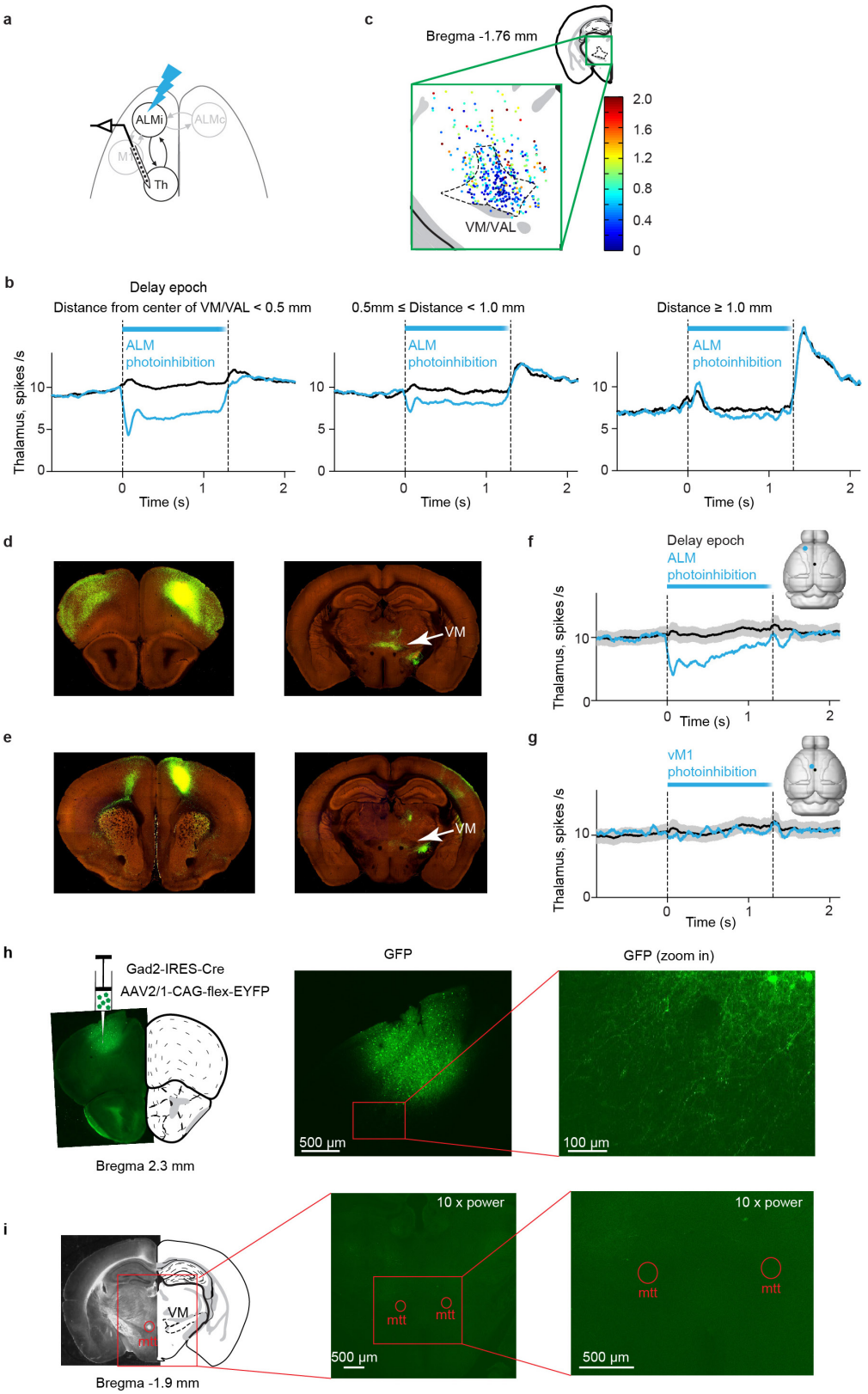

Extended Data Figure 8 | See next page for caption.

Extended Data Figure 8 | Modulation of thalamic activity by ALM photoinhibition is localized. a, VM/VAL recordings during ALM photoinhibition. **b**, PSTH of thalamic neurons averaged during control (black) and photoinhibition (light blue). Neurons were grouped by distance to the centre of VM/VAL. Distance <0.5 mm, $n=250$; $0.5 \leq$ distance < 1.0 mm, $n=160$; distance ≥ 1.0 mm, $n=46$. Averaging window, 100 ms. **c**, Locations of recorded neurons in the thalamus, projected to the example coronal section. Colour code shows the spike rate during ALM photoinhibition normalized to control (the first 100 ms of photoinhibition, see Methods). Same data as in Fig. 6d. **d**–**g**, Comparison of the effects of photoinhibition of ALM versus vM1 on VM/VAL activity. Labelling corticothalamic projections from ALM (data from mouse connectivity map of the Allen Brain Atlas ID 263242463, http://connectivity.brain-map.org/)[20] (see also Extended Data Figs 1, 9). **e**, Labelling corticothalamic projections from vM1 (data from mouse connectivity map of the Allen Brain Atlas ID 168162771)[20]. **f**, ALM photoinhibition. PSTH of VM/VAL neurons averaged during control (black) and ALM photoinhibition (blue). The s.e.m. was estimated by bootstrapping over neurons ($n=46$ cells from 3 mice.). The s.e.m. for photoinhibition conditions are not displayed for clarity. Averaging window, 100 ms. **g**, vM1 photoinhibition. PSTH of VM/VAL neurons averaged during control (black) and vM1 photoinhibition (blue) conditions. Photoinhibiting the vM1 produced a lower reduction in VM/VAL activity. The s.e.m. was estimated by bootstrapping over neurons ($n=46$ cells from 3 mice). The s.e.m. for photoinhibition conditions are not displayed for clarity. Averaging window, 100 ms. **h**, **i**, Absence of long-range GABAergic projections from the ALM in the thalamus. **h**, GABAergic neurons labelled with GFP in the ALM. Left, AAV2/1-CAG-flex-EGFP was injected into the ALM in a Gad2-IRES-Cre mouse. Middle, confocal images showing GABAergic neurons expressing EGFP. Same neurons as on the left. Right, magnified view of the boxed region in the middle, showing labelled axons of GABAergic neurons. **i**, Absence of GABAergic axons in the VM. Left, VM and the mammilothalamic tract (mtt). Middle, confocal image of the region on the left. Laser power was $10\times$ higher compared to **h**. Images were contrast-enhanced to show small structures. Right, magnified view of the indicated region in the middle. No labelled axonal processes were detected in the thalamus.

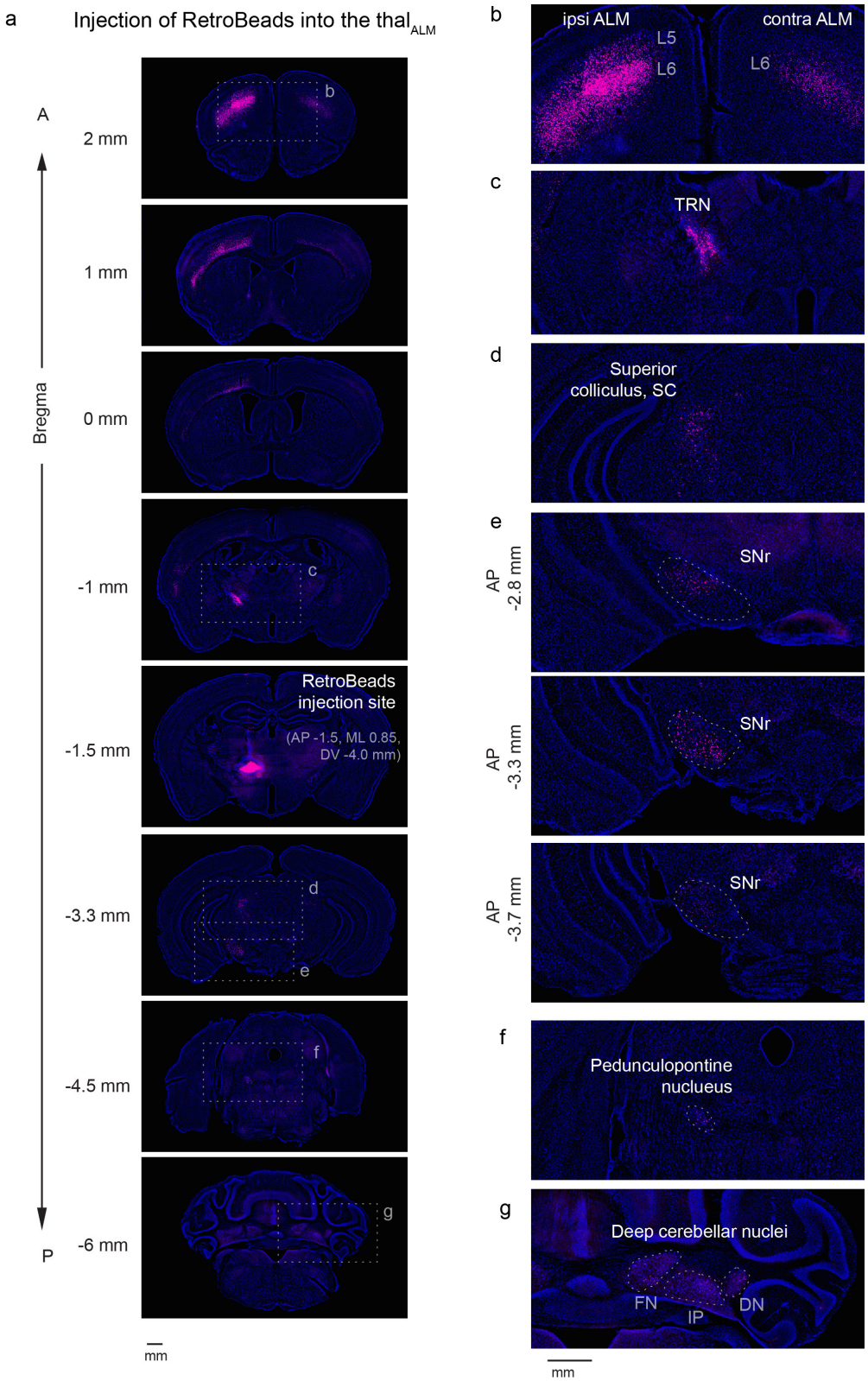

Extended Data Figure 9 | Thalamic regions that are connected reciprocally with the ALM (thal$_{ALM}$) receive input from multiple brain areas. RetroBeads were injected into the thal$_{ALM}$ (AP −1.5, ML 0.85, DV −4.0 mm from bregma, mainly in the VM). Magenta, retrograde labelling; blue, Nissl staining. **a**, Coronal sections. Dashed boxes indicate location of magnified images in **b**–**g**. **b**, Labelling in the ALM. Overall labelling was much stronger in the ipsilateral ALM. Labelling in the ALM was observed on both sides in L6, whereas labelling in L5 was seen only in the ipsilateral ALM. L6 neurons are corticothalamic neurons, whereas the L5 neurons correspond to pyramidal-tract neurons that send a branch to the thalamus[60]. In addition to the ALM, labelling was observed in M1, S2 and weakly in other cortical areas (see **a**). **c**, Labelling in the ipsilateral TRN. **d**, Labelling in the ipsilateral superior colliculus (SC). **e**, Labelling in the ipsilateral SNr, in three coronal sections. Labelling was observed throughout the SNr from the caudal to the rostral end, consistent with a previous report[54]. **f**, Labelling in the ipsilateral pedunculopontine nucleus (PPN). **g**, Labelling in the contralateral deep cerebellar nuclei. DN, dentate nucleus; FN, fastigial nucleus; IP, interposed nucleus.

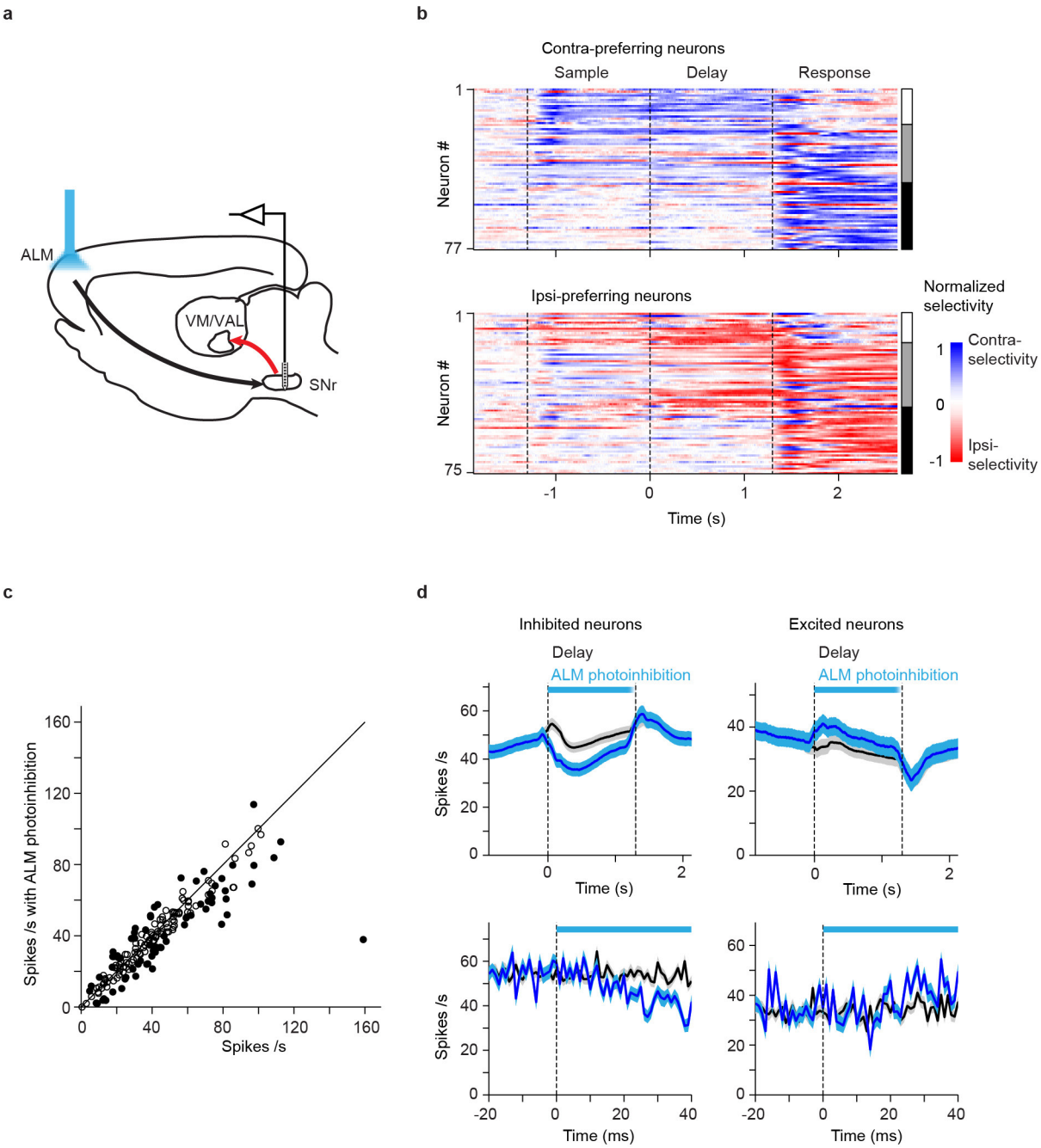

Extended Data Figure 10 | The effect of ALM photoinhibition on SNr activity. a, Schematic of SNr recording during ALM photoinhibition. Because the SNr→thalamus projection is inhibitory (red arrow), the SNr could contribute to VM/VAL inhibition, if ALM photoinhibition activates the SNr. We used multi-shank silicon probes (spanning 600 μm, medial to lateral) to survey a large part of the SNr (medial, lateral, rostral and caudal). **b**, SNr population selectivity. Selectivity is the difference in spike rate between the preferred and non-preferred trial type, normalized to the peak selectivity. Only putative GABAergic neurons with significant trial selectivity are shown ($n = 152$ out of 181, t-test, $P < 0.05$). The scale bar on the right indicates selectivity type: neurons showing preparatory activity only (white); both preparatory activity and peri-movement activity (grey); peri-movement activity only (black). Averaging window, 200 ms. SNr selectivity is similar to the ALM and VM/VAL (Fig. 2). **c**, Scatter plot of SNr GABAergic neurons ($n = 181$; spikes measured for 100 ms, starting 20 ms after photostimulus onset; Methods). Filled circles, neurons that were significantly modulated by ALM photoinhibition ($P < 0.05$, t-test). Photoinhibition of ALM changed only a relatively small fraction of SNr neurons (48 out of 181 significantly inhibited; 23 out of 181 significantly activated; $P < 0.05$, t-test). Moreover, neurons that decreased their activity were more numerous than neurons that increased their activity (bootstrapping over neurons; $P < 0.01$, Methods). Overall, inhibiting the ALM reduced SNr activity by 3.6 spikes per s (8.3% of control activity measured for 100 ms, starting 20 ms after photostimulus onset). This reduction in neural activity in the SNr is expected to increase thal_{ALM} activity. **d**, The time course of SNr GABAergic neurons during ALM photoinhibition. Left, significantly inhibited neurons ($n = 48$). Right, significantly excited neurons ($n = 23$). The s.e.m. was estimated by bootstrapping over neurons. Top, averaging window, 100 ms. Bottom, bin size, 1 ms. SNr neurons were affected by ALM photoinhibition with a relatively long latency difference (15.2 ± 4.6 ms (mean ± s.e.m.), $P < 0.05$, t-test), longer than for reducing thal_{ALM} activity (10.9 ± 2.9 ms; Fig. 6e). These data indicate that the ALM to SNr pathway does not contribute to the early phase of VM/VAL inhibition after ALM photoinhibition.